nature communications

Article

https://doi.org/10.1038/s41467-024-52379-2

FGF21 modulates immunometabolic homeostasis via the ALOX15/15-HETE axis in early liver graft injury

Received: 19 December 2023

Accepted: 2 September 2024

Published online: 03 October 2024

Check for updates

Xinyu Yang[1,2,12], Hao Chen[2,12], Wei Shen[2,12], Yuanming Chen[2,12], Zuyuan Lin[1,2], Jianyong Zhuo[1], Shuai Wang[1], Modan Yang[3], Huigang Li[2], Chiyu He[2], Xuanyu Zhang[4], Zhihang Hu[2], Zhengxing Lian[1], Mengfan Yang[5], Rui Wang[6], Changbiao Li[7], Binhua Pan[1], Li Xu[4], Jun Chen[7], Xuyong Wei[1], Qiang Wei[8], Haiyang Xie[9], Shusen Zheng[4,9,10], Di Lu[7,9] ✉ & Xiao Xu[8,9,11] ✉

Fibroblast growth factor 21 (FGF21) is essential for modulating hepatic homeostasis, but the impact of FGF21 on liver graft injury remains uncertain. Here, we show that high FGF21 levels in liver graft and serum are associated with improved graft function and survival in liver transplantation (LT) recipients. FGF21 deficiency aggravates early graft injury and activates arachidonic acid metabolism and regional inflammation in male mouse models of hepatic ischemia/reperfusion (I/R) injury and orthotopic LT. Mechanistically, FGF21 deficiency results in abnormal activation of the arachidonate 15-lipoxygenase (ALOX15)/15-hydroxy eicosatetraenoic acid (15-HETE) pathway, which triggers a cascade of innate immunity-dominated pro-inflammatory responses in grafts. Notably, the modulating role of FGF21/ALOX15/15-HETE pathway is more significant in steatotic livers. In contrast, pharmacological administration of recombinant FGF21 effectively protects against hepatic I/R injury. Overall, our study reveals the regulatory mechanism of FGF21 and offers insights into its potential clinical application in early liver graft injury after LT.

Liver transplantation (LT) is a life-saving intervention for patients with end-stage liver diseases. However, early allograft dysfunction (EAD) is a serious complication of post-transplant early graft injury, and it affects approximately one-fourth of liver recipients and portends poor allograft and patient survival[1–3]. Ischemia-reperfusion (I/R) injury is a leading cause of EAD and a major determinant of the severe organ shortage for transplantation[4,5]. The increasing gap between the demand and supply of organs in recent decades has extended the interest in using expanded criteria donors to expand the liver donor pool, including steatotic donor livers[6]. Steatotic livers are more prone to I/R injury, which increases the risk of organ dysfunction or failure[7,8]. Despite its clinical importance, the underlying mechanisms of early graft injury are only partially understood[4]. Pharmacological interventions for precise prevention and novel

[1]Key Laboratory of Integrated Oncology and Intelligent Medicine of Zhejiang Province, Hangzhou First People's Hospital, Hangzhou, China. [2]Zhejiang University School of Medicine, Hangzhou, China. [3]Department of Breast Surgery, The Second Affiliated Hospital, Zhejiang University School of Medicine, Hangzhou, China. [4]Department of Hepatobiliary and Pancreatic Surgery, The First Affiliated Hospital, Zhejiang University School of Medicine, Hangzhou, China. [5]Department of Organ Transplantation, Qilu Hospital of Shandong University, Jinan, China. [6]Liangzhu Laboratory, Zhejiang University Medical Center, Hangzhou, China. [7]Department of Hepatobiliary & Pancreatic Surgery and Minimally Invasive Surgery, Zhejiang Provincial People's Hospital (Affiliated People's Hospital), Hangzhou Medical College, Hangzhou, China. [8]School of Clinical Medicine, Hangzhou Medical College, Hangzhou, China. [9]NHC Key Laboratory of Combined Multi-organ Transplantation, Hangzhou, China. [10]Department of Hepatobiliary and Pancreatic Surgery, Shulan (Hangzhou) Hospital, Hangzhou, China. [11]Institute of Translational Medicine, Zhejiang University, Hangzhou, China. [12]These authors contributed equally: Xinyu Yang, Hao Chen, Wei Shen, Yuanming Chen. ✉e-mail: zjludi@zju.edu.cn; zjxu@zju.edu.cn

strategies to alleviate graft injury and improve functional recovery are urgently needed.

As an endogenous metabolic regulator, fibroblast growth factor 21 (FGF21) is produced mostly in the liver to mediate metabolic homeostasis[9]. Pharmacological administration of FGF21 can produce favorable effects, including lipid-lowering, weight-reducing, and anti-diabetic effects[10]. A phase 2 trial reported that pegbelfermin (BMS-986036), which is a polyethylene glycol-conjugated (PEGylated) recombinant analog of human FGF21, improved a variety of metabolic parameters and reduced hepatic steatosis in patients with nonalcoholic steatohepatitis (NASH)[11]. Previous research has mainly focused on its roles related to energy, glucose/lipid metabolism, and insulin sensitivity. FGF21 also elicits protective effects against certain acute diseases, including acute liver injury, myocardial infarction, and stroke[10,12]. Moreover, FGF21 is closely involved in the progression of acute-on-chronic liver failure and has a great predictive potential for organ failure[13]. However, it remains unclear whether the modulating role of FGF21 provides a benefit to graft function after LT or the specific underlying molecular mechanism involved.

Lipoxygenases (LOXs) are non-heme iron enzymes that catalyze the peroxidation of polyunsaturated fatty acids (PUFAs), producing hydroperoxy derivatives. They act as pro- and anti-inflammatory mediators and are involved in membrane restructuring, lipoprotein interaction, and cellular redox regulation[14,15]. Arachidonate 15-lipoxygenase (*ALOX15*), encoding 15-LOX (also known as 12-LOX or 12/15-LOX), utilizes natural substrates like arachidonic acid (AA), docosahexaenoic acid, *et al*. These substrates are present either in their free state or integrated into molecules like phospholipids, glycerides, or cholesterol esters[16]. 15-hydroxyeicosatetraenoic acid (15-HETE) is converted by *ALOX15* from AA, a prominent ω−6 PUFA representing a major component of the cell membrane phospholipids and the metabolic precursor of eicosanoids[16]. These compounds are then metabolized into diverse bioactive molecules, contributing to the pathogenesis of several diseases[16,17]. Some studies have reported that *Alox15* deficiency, which lowers plasma 15-HETE levels, protects against steatohepatitis, hyperlipidemia, and alcoholic liver disease (ALD) by reducing reactive oxygen species (ROS) production, hepatic steatosis, insulin resistance, and inflammatory injury[18–21]. ALOX15 was also found to be highly expressed in human ischemic heart tissue[22]. Croon et al. further discovered that the metabolic adaptation to mitochondrial dysfunction in cardiomyocytes is strongly blunted due to the absence of FGF21, resulting in a significant upregulation of ALOX15[23]. However, the role of ALOX15 in the pathogenesis of ischemic liver disease remains unknown. Additionally, the molecular mechanisms behind FGF21 and ALOX15 need to be elucidated.

In this study, we hypothesized that the FGF21 signaling pathway would be part of a protective response against inflammatory graft injury following LT, possibly through the suppression of the ALOX15/15-HETE axis. Based on clinical samples, in vivo and in vitro models, the present study identified FGF21 as a valuable marker for transplanted liver graft injury and a potent modulator of hepatic metabolism and immunological response, especially in transplants using steatotic livers. Collectively, our findings offer further insights into a potential therapeutic intervention against sterile inflammatory liver injury.

Results

FGF21 expression was closely correlated with clinical outcomes after LT

The general workflow is shown schematically in Fig. 1a. Analysis of GSE15480 (n = 12) and GSE151648 (n = 40) showed that the hepatic expression of *FGF21* was significantly elevated post-transplantation ($p = 0.0172$ and $p = 0.0003$, respectively, Fig. 1b). For the 88 transplants in Cohort 1 (with pre- and post-reperfusion serum samples), the baseline characteristics and clinicopathological features are shown in Supplementary Table 1. We observed a significant increase in FGF21 in the serum 2 h after reperfusion ($p = 0.0018$, Fig. 1c). Notably, serum FGF21 after reperfusion negatively correlated with the peak ALT level within 7 d after transplantation ($p = 0.0354$, Fig. 1d). These patients were divided into the serum FGF21-elevated group (n = 44) and the non-elevated group (n = 44) according to the median value of ratio change (post-reperfusion/pre-transplant). The peak AST level within 7 d after transplantation was decreased in the elevated group ($p = 0.0305$, Supplementary Fig. 1a). Survival analysis also indicated that the elevated group had improved graft survival ($p = 0.0159$, Fig. 1e). High mobility group box 1 (HMGB1), reported as an indicator of cell injury, was found to have a positive association with peak ALT levels within 7 days after transplantation ($p = 0.0217$, Supplementary Fig. 1b). Notably, the peripheral FGF21 level was negatively correlated with the peripheral HMGB1 level 2 hours after reperfusion ($p = 0.0296$, Supplementary Fig. 1c).

FGF21 protein levels were determined using IHC in the 115 liver graft biopsies from Cohort 2 (during preservation). The baseline characteristics and clinicopathological features are shown in Supplementary Table 2. After excluding liver grafts with CIT > 15 h, 107 patients were analyzed. Using a quantitative score of 8 as the threshold, these patients were divided into a low FGF21 group (n = 42) and a high FGF21 group (n = 65) (Fig. 1f). Survival analysis showed that high FGF21 was associated with improved graft survival ($p = 0.035$, Fig. 1g). As documented by the transplant center, 33 patients received steatotic liver grafts in this cohort. Low FGF21 in the graft was associated with elevated ALT ($p = 0.0495$) and AST ($p = 0.0465$) after transplantation in this subgroup (Fig. 1h). However, there was no significant difference in non-steatotic grafts. We also observed a potential increase in the incidence of EAD in the low FGF21 grafts compared to the high FGF21 grafts (73.3% vs. 50.0%) in the group of steatotic grafts, but there was no statistical significance (Supplementary Fig. 1d).

FGF21 deficiency aggravates hepatic I/R injury

The protein level of FGF21 was upregulated after reperfusion in the mouse model of hepatic I/R injury and peaked at 6 h (Fig. 2a). To examine the function of FGF21 in hepatic I/R injury, we subjected *Fgf21* KO mice and wild-type controls to 1.5 h of hepatic ischemia followed by reperfusion for 6 h (Fig. 2b). As shown in Fig. 2c, FGF21 deficiency significantly aggravated the I/R-induced elevation of serum ALT and AST. FGF21 deficiency also greatly increased liver damage and hepatocellular necrosis (Fig. 2d, e). Compared to the wild-type mice, the number of apoptotic cells was also significantly increased in the livers of *Fgf21* KO mice, as demonstrated by TUNEL staining (Fig. 2f, g).

FGF21 deficiency exacerbates I/R-induced inflammation via the ALOX15/15-HETE axis

To elucidate the underlying mechanism of hepatic I/R injury driven by FGF21 deficiency, we performed RNA-Seq of I/R-treated liver samples from *Fgf21* KO and wild-type mice. Profiling of the differentially expressed genes (DEGs) showed that lipid metabolism was dramatically different between the 2 groups, particularly the arachidonic acid (AA) metabolism pathway (Fig. 2h, i). Therefore, we also performed lipidomic analysis on liver tissues, a total of 42 lipid classes were identified. Analysis of the differentially expressed metabolites highlighted AA metabolism as the enriched changed pathway (Fig. 2j). Combined with Fig. 2k, we noticed that 15-HETE, which is involved in the AA pathway, was one of the most upregulated metabolites in *Fgf21* KO livers after I/R treatments. Weighted gene co-expression network analysis (WGCNA) showed the gene/metabolite modules that were closely related to *Alox15* or 15-HETE (Fig. 2l). Various inflammatory signaling pathways were enriched in the module with the highest degree of positive correlation, which indicated the potential role of ALOX15/15-HETE in modulating I/R-induced hepatic inflammation. To confirm the correlation with clinical outcome, ALOX15 protein levels were determined using IHC in pre-transplant liver graft biopsies from

https://doi.org/10.1038/s41467-024-52379-2

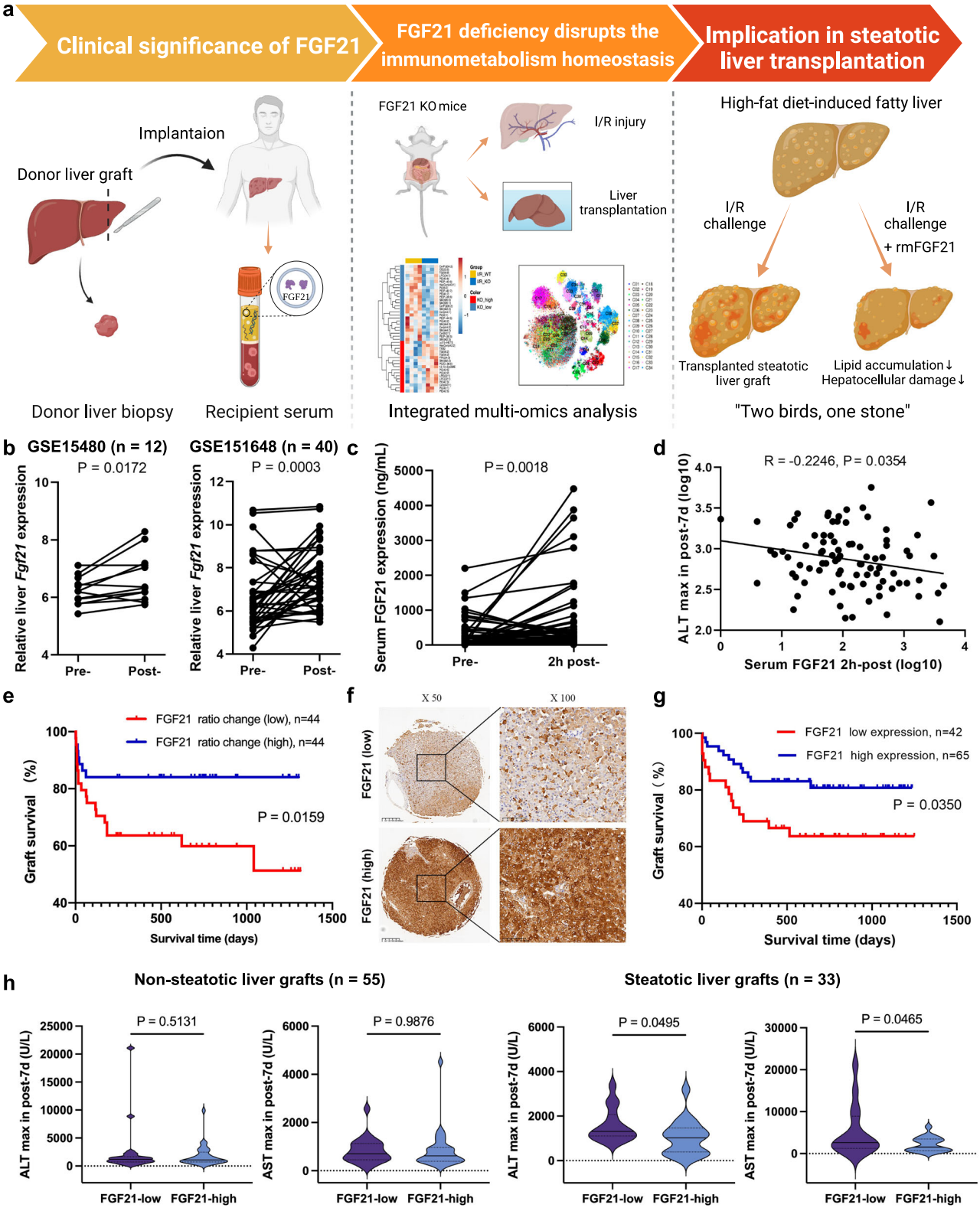

Cohort 2. According to the average integrated optical density (IOD) of IHC staining, the 115 cases were divided into a low ALOX15 group and a high ALOX15 group (Supplementary Fig. 2a). The high ALOX15 grafts had a significantly higher incidence of EAD than the low ALOX15 grafts (41.4% vs. 22.8%, $p = 0.0330$) (Supplementary Fig. 2b).

Because of the critical effect of the ALOX15/15HETE axis, we examined whether 15-HETE production affected I/R injury. An ALOX15 inhibitor, PD146176[24], and 15-HETE were used to modulate 15-HETE content in mouse I/R models (Fig. 3a). Significantly decreased 15-HETE was detected in PD146176-treated livers after I/R treatment (Fig. 3b). Mice treated with PD146176 had decreased ALT/AST levels and less necrosis on H&E staining, and mice treated with 15-HETE exhibited more severe liver injury (Fig. 3c, d). We also detected significantly lower ROS production, inflammatory cell infiltration and apoptosis in the PD146176-treated livers, and the exact opposite effects were observed in the 15-HETE-treated livers (Fig. 3d). To further validate that

Fig. 1 | The general workflow and the association of FGF21 expression with clinical outcomes. a An overview of a general workflow for the study. **b** Comparison of pre- and post-transplantation *Fgf21* mRNA expression in the liver graft based on the GSE15480 (n = 12 pairs, including pre- and post-LT donor livers) and GSE151648 (n = 40 pairs, including pre- and post-LT donor livers) derived from graft biopsies in liver transplantation. **c** Comparison of pre- and post-reperfusion FGF21 levels in the serum (Cohort 1, n = 88 pairs, including pre- and 2 h post-LT recipient serum). **d** The peripheral FGF21 level 2 h after reperfusion linearly correlated with maximal ALT within 7 days after transplantation. **e** The 88 patients were divided into the FGF21-elevated group (n = 44) and non-elevated group (n = 44) according to the median value of ratio change (post-reperfusion/pre-transplant). The elevated group had improved graft survival. **f**, **g** Pre-transplant FGF21 expression in biopsies (Cohort 2, n = 115) and its correlation with graft survival (after excluding liver grafts with CIT > 15 h, n = 107). **h** Information on graft steatotic change was missing for 19 cases in this cohort. We confirmed that 33 patients received steatotic liver grafts. Low FGF21 in the graft was associated with elevated ALT and AST after transplantation. However, there was no significant difference in the non-steatotic subgroup (n = 55). I/R, ischemia/reperfusion; KO knockout, ALT alanine aminotransferase, AST aspartate aminotransferase, CIT cold ischemia time. *p* values are shown on the graphs. Source data are provided as a Source Data file. Figure 1a created with BioRender. com released under a Creative Commons Attribution-NonCommercial-NoDerivs 4.0 International license (https://creativecommons.org/licenses/by-nc-nd/4.0/deed.en).

I/R injuries in *Fgf21* KO mice are due to ALOX15 increase, ALOX15 inhibitor was used in *Fgf21* KO mice (Supplementary Fig. 3a). *Fgf21* KO mice treated with PD146176 also showed decreased ALT/AST levels and less necrosis on H&E staining (Supplementary Fig. 3b, c). Reduced apoptosis and inflammatory cell infiltration were also observed in the PD146176-treated *Fgf21* KO livers (Supplementary Fig. 3d, e).

We also established transgenic mouse models of liver-specific *Alox15* knockdown (*Alox15*-KD) using transfection with AAV8-TBG-*Alox15* shRNA (Supplementary Fig. 4a). *Alox15*-KD in the liver produced resistance to I/R injury, which was demonstrated as improved liver function and alleviation of histopathological liver damage (Supplementary Fig. 4b–e). Taken together, these observations revealed the regulatory role of the FGF21/ALOX15/15-HETE axis in hepatic I/R injury.

FGF21 deficiency enhances the innate immune response in transplanted livers

We further established mouse models of orthotopic LT using wild-type (WT) and *Fgf21* knockout (KO) mice (Fig. 4a) and performed multiplex analysis of inflammatory cytokines and CyTOF on the transplanted liver grafts. As shown in Fig. 4b, c, serum ALT, AST, and hepatic 15-HETE were significantly elevated in WT mice that received *Fgf21* KO liver grafts. As expected, serum FGF21 in the sham group of *Fgf21* KO mice was completely depleted. Meanwhile, a significantly decreased serum FGF21 level was found in WT mice that received *Fgf21* KO liver grafts compared to *Fgf21* KO mice that received WT liver grafts (Fig. 4d). TUNEL staining also showed an increased frequency of apoptotic cells in transplanted *Fgf21* KO liver grafts (Fig. 4e). Pro-inflammatory cytokines, such as CCL-5, TNF-α, IL-9 and GM-CSF, increased significantly in the *Fgf21* KO liver grafts, and peripheral TNF-α and IL-17 were reduced (Supplementary Fig. 5a). Next, more than 4 million immune cells were analyzed using CyTOF. The collected data were gated to exclude residual normalization beads, debris, dead cells and doublets, leaving live $CD45^+$ events for subsequent clustering and high-dimensional analyses (Supplementary Fig. 5b). Then, 34 clusters were identified (Fig. 4f). Notably, granulocytes, mono/mac and NK cells were predominantly elevated in *Fgf21* KO liver grafts after transplantation (Fig. 4g). Typical subsets of granulocytes and mono/mac cells that were increased in *Fgf21* KO liver grafts are shown in Fig. 4h, i. Notably, we also identified a predominant cluster of NK cells, $CD62L^+$ NK cells, in *Fgf21* KO liver grafts (Fig. 4j). CD62L is a mediator of leukocyte homing to inflamed sites[25]. Immunofluorescence showed that $CD62L^+$ NK cells primarily accumulated around the peripheral portal vein (Fig. 4k), which indicated their recruitment from peripheral blood into the transplanted liver. These results suggest that an excessive innate immune response was induced in *Fgf21* KO liver grafts after transplantation, which contributed to the exacerbation of liver injury.

Pharmacological administration of rmFGF21 activates the FGFR4-ERK1/2 pathway to ameliorate I/R-induced pathologies

We administered rmFGF21 prior to I/R treatment in mice to study its curative effect on hepatic injury (Fig. 5a). Compared to the control mice, the serum levels of ALT and AST in the rmFGF21 group were significantly decreased 6 h after reperfusion (Fig. 5b). I/R groups displayed a significant increase in serum FGF21 levels compared to the sham group (Fig. 5c). Moreover, the rmFGF21 group demonstrated the highest serum FGF21 levels after I/R. rmFGF21-treated mice also exhibited resistance to I/R injury, as demonstrated by decreased sinusoidal congestion, edema and vacuolization or necrosis (Fig. 5d) and a reduced frequency of TUNEL-positive cells (Supplementary Fig. 6a). Western blotting also identified elevated anti-apoptotic protein BCL-2, reduced pro-apoptotic protein C-caspase3 and ALOX15 in the livers of the rmFGF21 group (Supplementary Fig. 6b).

To evaluate the putative mechanisms in a cell-type specific manner, we assessed the modulatory function of rmFGF21 in H/R-stressed murine hepatocyte cultures. We observed increased FGF21 expression and apoptosis in AML12 after H/R treatment (Fig. 5e). The phosphatidylinositol-3-kinase (PI3K)/AKT and extracellular signal-regulated protein kinases 1 and 2 (ERK1/2) pathways are well known to be regulated by FGF21, which are involved in regulating various metabolic processes[10,26]. To determine whether the ERK1/2 pathway is downstream of rmFGF21, we analyzed the phosphorylation levels of ERK1/2 and found that rmFGF21 treatment increased the phosphorylation. Meanwhile, rmFGF21 also reduced the levels of ALOX15 while activating the ERK1/2 pathway, and such effects were diminished by treatment with an ERK1/2 specific inhibitor SCH772984 (Fig. 5f). By contrast, inhibition by a PI3K specific inhibitor LY294002 had no such effects (Supplementary Fig. 6c). FGF receptors (FGFRs), mainly FGFR4, which is expressed in liver, and FGFR1, which is predominantly expressed in adipose tissues, are considered the primary mediators of the metabolic effects of FGF21 and FGF19[27]. To distinguish which FGFRs mediate the activation of the ERK1/2 pathway and the inhibition of ALOX15 induced by rmFGF21, we used selective FGFR1 tyrosine kinase inhibitor PD166866. We found that rmFGF21 retained the inhibitory effect on apoptosis under these conditions (Supplementary Fig. 6d), indicating that hepatic FGFR1 likely does not mediate the protective activity of rmFGF21. By contrast, the phosphorylation of FGFR4 and the inhibition of ALOX15 induced by rmFGF21 were abolished by treatment with the FGFR4-specific inhibitor FGF401 (Fig. 5g). These data indicated that hepatic FGFR4, but not FGFR1, mediates the protective effect of rmFGF21.

FGF21 expression was associated with clinical outcomes in LT using steatotic grafts

Because FGF21 is a major regulator of hepatic lipid metabolism, we suspected that it played a role in decreasing the susceptibility of steatotic liver grafts to I/R injury. For the 78 transplants using steatotic liver grafts in Cohort 3, baseline characteristics and clinicopathological information are shown in Supplementary Table 3. According to the average IOD of IHC staining, the 78 cases were divided into a low FGF21 group and a high FGF21 group (Fig. 6a). No significant difference was found in the analysis comparing the degree of hepatic steatosis between these two groups (Fig. 6b). Low expression of FGF21 in the donor grafts indicated higher peaks of ALT ($p = 0.0027$) and AST ($p = 0.0064$) within the first 7 days after transplantation (Fig. 6c).

https://doi.org/10.1038/s41467-024-52379-2

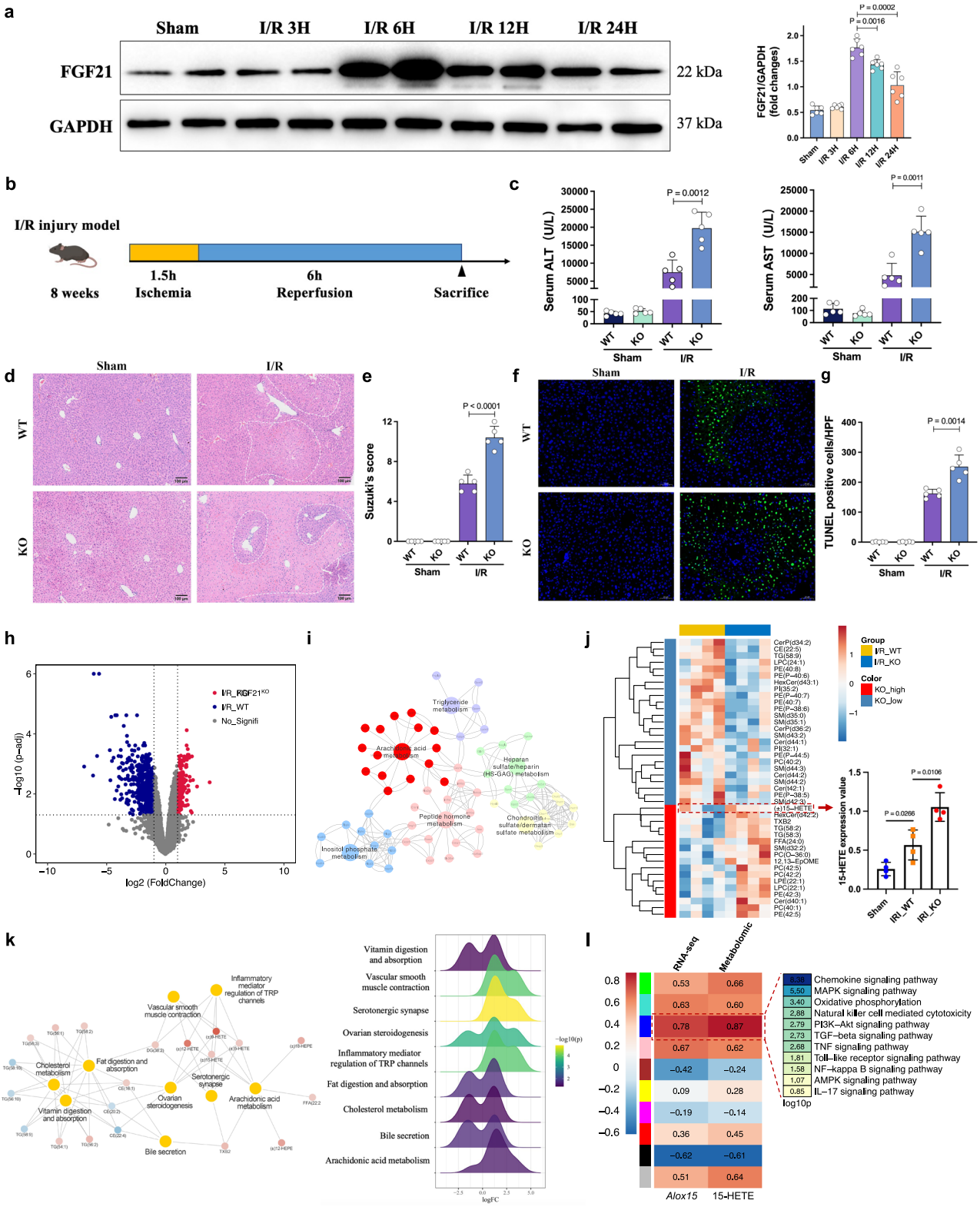

Comparison of the EAD and non-EAD patients showed that the IOD of FGF21 staining was also significantly lower in the grafts that developed EAD after transplantation ($p < 0.0001$, Fig. 6d).

FGF21 deficiency aggravates susceptibility to I/R injury in steatotic livers

We established a steatotic liver I/R injury model using mice fed a high-fat diet (HFD) for 8 weeks (Fig. 6e). I/R injury appeared more severe in the steatotic liver, and FGF21 deficiency significantly increased serum ALT and AST after I/R treatment in the steatotic livers (Fig. 6f). We detected significantly higher 15-HETE levels in HFD-fed *Fgf21* KO livers after I/R injury (Fig. 6g). Considerably increased hepatic necrosis, ROS production and apoptotic cells were observed in the liver sections of HFD-fed *Fgf21* KO mice compared to the HFD-fed wild-type mice (Fig. 6h). HFD-fed *Fgf21* KO livers had increased intrahepatic infiltration of $CD11b^+$ and cytosolic myeloperoxidase (MPO) positive cells

Fig. 2 | FGF21 deficiency aggravated I/R-induced liver injury. a The time-dependent western blot analysis (left) and quantification (right) of FGF21 protein expression in the mouse liver undergoing ischemia for 1.5 h followed by the indicated duration of reperfusion, three independent biological mice samples. **b** Schematic for the establishment of the mouse I/R injury model. **c** Serum ALT and AST levels of wild-type and *Fgf21* KO mice in the sham and I/R groups 6 h after reperfusion (n = 5, per group). **d** Representative H&E staining of liver sections from wild-type and *Fgf21* KO mice in the sham and I/R groups. **e** Liver damage was evaluated using Suzuki's histological score (n = 5, per group). **f** Representative TUNEL immunofluorescent staining in liver lobes of wild-type and *Fgf21* KO mice in the sham and I/R groups. **g** Quantification analysis of the TUNEL-positive cells/high-power field (n = 5, per group). **h** Volcano plot of the differentially expressed genes (DEGs) between wild-type and *Fgf21* KO livers after I/R treatment (n = 4) using the absolute value of log2 (fold change) >1.5 and $p < 0.05$ as the thresholds. **i** KEGG pathway enrichment analysis of the identified DEGs. **j** Heatmap of major metabolites catalyzed by lipoxygenases in wild-type and *Fgf21* KO livers after I/R treatment (n = 4). The 15-HETE content was elevated in *Fgf21* KO livers. **k** Co-expression network and KEGG pathway analysis of the hub metabolites. **l** The Pearson correlation coefficients between ALOX15/15-HETE (RNA-seq/metabolomic) and the co-expression modules identified by WGCNA. KEGG analysis of the module with the highest correlation coefficients ($p < 0.05$ by Fisher's exact test, two-sided). WT, wild-type, KO knockout, I/R ischemia/reperfusion, ALT alanine aminotransferase, AST aspartate aminotransferase. **a**, **c**, **e**, **g**, **j** Two-tailed *t* test. Statistic data are presented as the mean ± SD, error bars represent the means of at least three independent experiments. *p* values are shown on the graphs, $p < 0.05$ was considered statistically significant. Source data are provided as a Source Data file. Figure 2b created with BioRender. com released under a Creative Commons Attribution-NonCommercial-NoDerivs 4.0 International license (https://creativecommons.org/licenses/by-nc-nd/4.0/deed.en).

compared to wild-type controls after I/R injury (Fig. 6i). HFD-fed *Fgf21* KO livers also showed mild to severe hepatosteatosis after I/R injury, with clustered and ballooning lipid macrovesicles, and wild-type livers after I/R injury predominantly exhibited dispersed lipid microvesicles (Supplementary Fig. 7a, b). Serum TG levels were also higher in HFD-fed *Fgf21* KO mice (Supplementary Fig. 7c). These data indicated the role of FGF21 in regulating the immunometabolism of steatotic livers after I/R treatments.

The ALOX15/15HETE axis in I/R injury in steatotic livers

To verify the essential role of ALOX15 in I/R injury in steatotic livers, we established two types of models using transfection with AAV8-TBG-*Alox15* shRNA (liver-specific knockdown) or intraperitoneal administration of PD146176 before I/R treatment in HFD mice (Fig. 7a). We observed a decrease of 15-HETE content in the *Alox15*-KD steatotic livers (Fig. 7b). The *Alox15*-KD steatotic livers showed higher resistance to I/R injury, which was demonstrated as improved liver function and alleviated histopathological liver damage (Fig. 7c–e). The *Alox15*-KD steatotic livers had reduced intrahepatic infiltration of $CD11b^+$ and MPO^+ cells (Fig. 7f). Moreover, no significant change in steatosis and lipid accumulation was found in HFD-fed mice between with and without shAlox15 either in sham or I/R groups (Supplementary Fig. 8a–c).

Administration of PD146176 also decreased 15-HETE in the steatotic liver after I/R treatment (Fig. 7g). PD146176 significantly alleviated I/R injury in steatotic livers, which was demonstrated by improved liver function and attenuated histopathological changes (Fig. 7h–j). The PD146176-treated livers had reduced intrahepatic infiltration of $CD11b^+$ and MPO^+ cells (Fig. 7k).

The protective roles of FGF21 against I/R injury of steatotic livers

We developed two other types of mouse models using transfection with AAV8-hAAT-*Fgf21* (liver-specific overexpression) or intraperitoneal administration of rmFGF21 before the I/R procedure in HFD mice (Fig. 8a). Both treatment groups had significantly decreased 15-HETE in I/R-insulted livers and decreased ALT and AST in serum (Fig. 8b, c). Considerably attenuated hepatic necrosis, ROS production and TUNEL-positive cells were observed in the treatment groups (Fig. 8d). The *Fgf21*-overexpressing livers or rmFGF21-treated livers had reduced infiltration of $CD11b^+$ and MPO^+ inflammatory cells after I/R treatment (Fig. 8e). The two treatment groups had less steatotic changes compared to the control group (Supplementary Fig. 9a, b), and the serum TG level was also significantly lower (Supplementary Fig. 9c). These results demonstrated that transgenic overexpression of hepatic *Fgf21* or administration of rmFGF21 attenuated liver injury, apoptosis and inflammation after I/R in steatotic livers. Furthermore, a clear reversal of steatotic change was also achieved. The general schematic diagram is shown in Fig. 8f.

Moreover, we also administered one single dose of rmFGF21 prior to I/R treatment in HFD-fed mice to study its curative effect on steatotic liver injury (Supplementary Fig. 10a). Compared to the control mice, rmFGF21-treated mice exhibited a decreased serum ALT and AST after I/R injury in the steatotic livers (Supplementary Fig. 10b). Also, a significant decrease in hepatic necrosis, apoptotic cells and $CD11b^+$ cells were observed in the liver sections of rmFGF21 treatment mice compared to control mice (Supplementary Fig. 10c). However, no significant change in steatosis was found in HFD-fed mice with a single dose of rmFGF21 compared to the control group (Supplementary Fig. 10d, e).

Discussion

LT is currently considered the standard treatment for end-stage liver disease[28]. Early graft injury after LT is a pathological state initiated by I/R, can lead to impaired graft function, including EAD, which has a negatively impact on the survival of allografts and recipients[2,4]. Indeed, by contributing to the shortage of liver grafts, early graft injury represents one of the most significant challenges in LT[29]. Thus, novel therapeutic strategies to prevent I/R injury are needed to improve LT outcomes and expand the donor liver pool.

Hepatic FGF21 is a key endocrine factor that maintains metabolic homeostasis[9]. Accumulated evidence suggests that FGF21 exhibits potential therapeutic effects in ischemic injury of organs, such as the heart[30], skeletal muscle[31], and brain[32]. FGF21 is primarily expressed by the liver, and most circulating FGF21 comes from the liver[33,34]. Ye et al. reported that circulating FGF21 was elevated after hepatic reperfusion in LT[35]. In the present study, we observed that FGF21 was elevated in serum and donor liver tissues after reperfusion. Notably, the dramatic elevation of serum FGF21 occurred within the first 2 h after reperfusion, which was earlier than the major increase in serum ALT and AST levels. Our analysis of a limited sample size (n = 55) revealed that the levels of AST and ALT after transplantation are not affected by the levels of FGF21 in pre-transplant non-steatotic donor livers. This finding suggests that factors other than pre-transplant FGF21 expression may contribute more prominently to post-transplant AST and ALT levels in this specific context. However, considering all the present clinical correlation analyses, it is suggested that assessing post-transplant FGF21 levels or dynamic change between pre- and post-transplant would provide a more comprehensive understanding of FGF21 as a potential marker for transplanted liver graft injury.

Although our clinical findings suggested that the dramatic elevation of FGF21 exerted a protective adaptive response, and the deficiency of FGF21 contributed to graft injury, the underlying mechanisms were needed to be elucidated. During the process of I/R, a burst of ROS production in the liver activates the release of harmful products, which is termed damage-associated molecular patterns (DAMPs)[36]. The released DAMPs from stressed hepatocytes further trigger the release of chemokines and other mediators to elicit interconnected inflammatory cascades that exacerbate hepatocellular damage[37]. ALOX15 and its metabolites have a significant impact in the

https://doi.org/10.1038/s41467-024-52379-2

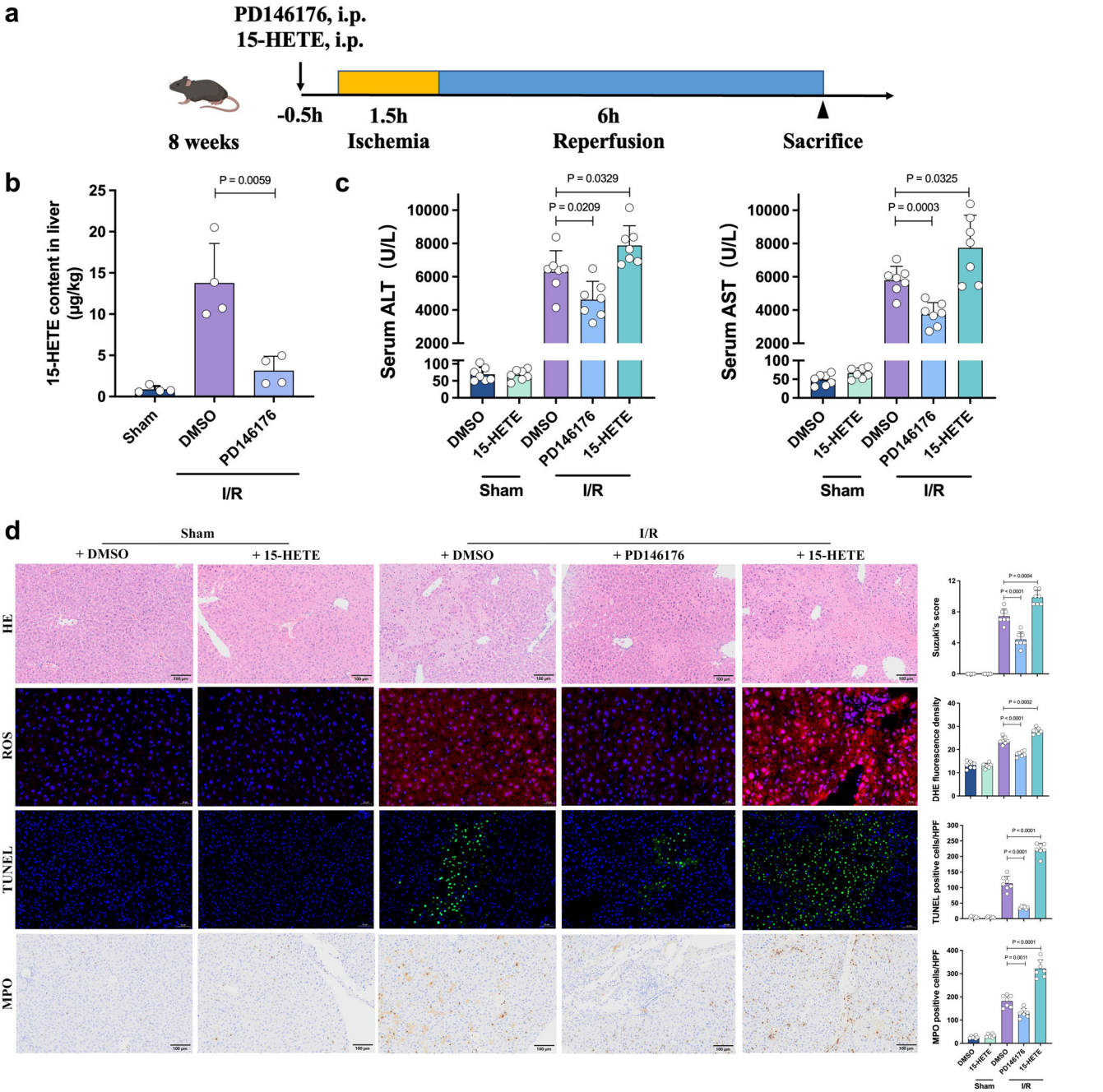

Fig. 3 | The regulatory role of ALOX15/15-HETE in the setting of hepatic I/R injury. a The experimental schema for establishing the mouse I/R injury model. The mice were intravenously administered PD146176 (10 mg/kg) or 15-HETE (0.5 mg/kg). **b** The 15-HETE level in the livers of each group 6 h after reperfusion (n = 4, per group). **c** Serum ALT and AST levels for each group 6 h after reperfusion (n = 7, per group). **d** Representative H&E staining, ROS staining, TUNEL staining and MPO IHC staining of liver sections from each group and quantification assessment (n = 7, per group). I/R, ischemia/reperfusion, ALT alanine aminotransferase, AST aspartate aminotransferase, HE hematoxylin and eosin, ROS reactive oxygen species, DHE dihydroethidium, TUNEL Terminal deoxynucleotidyl transferase dUTP nick end labeling, MPO cytosolic myeloperoxidase. Two-tailed t-test. Statistic data are presented as the mean ± SD, error bars represent the means of at least three independent experiments. *p* values are shown on the graphs, $p < 0.05$ was considered statistically significant. Source data are provided as a Source Data file. Figure 3a created with BioRender. com released under a Creative Commons Attribution-NonCommercial-NoDerivs 4.0 International license (https://creativecommons.org/licenses/by-nc-nd/4.0/deed.en).

fate of hepatic pathologies. Queck et al. showed that the lack of *Alox15* worsened parameters of liver disease and increased hepatic neutrophil and $CD4^+$ regulatory T-cells infiltration in alcoholic hepatitis, while Lipoxin A4 injection attenuated these parameters of disease progression in *Alox15*$^{-/-}$ mice[38]. However, Zhang et al. found that activation of ALOX15/13-hydroxyoctadecadienoic acid (13-HODE) circuit critically mediates the pathogenesis of ALD, *Alox15* knockout ameliorates alcohol-induced ROS production, endoplasmic reticulum stress, apoptosis, and liver injury[21]. Their data suggested that ALOX15 is a potential molecular target for treatment of ALD.

Different from the mechanism in ALD, our present study was able to define that ALOX15 was an important mediator of graft injury and noticed that 15-HETE, which is involved in the AA pathway, was one of the most upregulated metabolites in *Fgf21* KO livers after I/R treatments. Consistent with Wang et al.'s data showing that an ALOX15 inhibitor reduced macrophage recruitment and inflammation in

https://doi.org/10.1038/s41467-024-52379-2

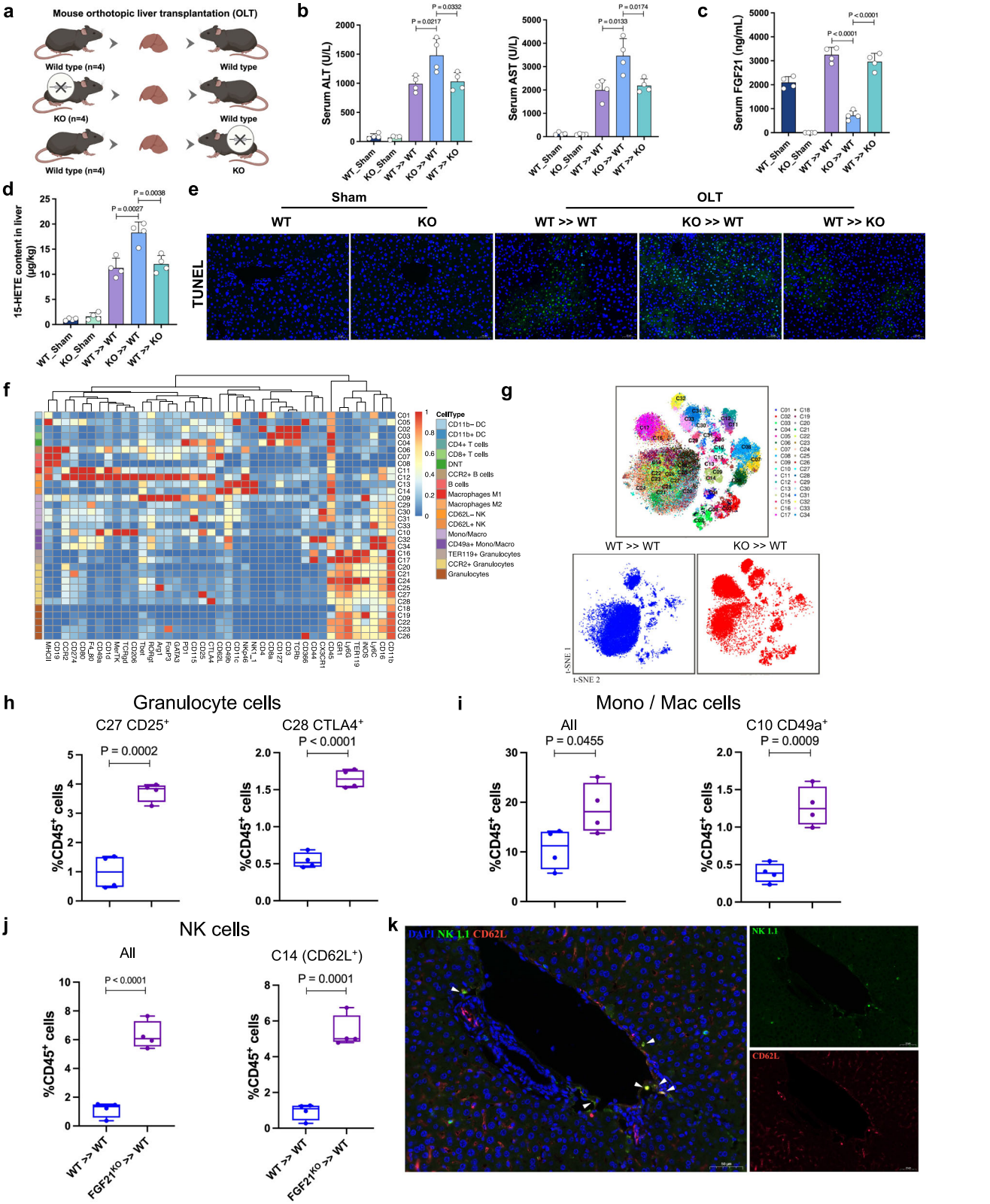

mice[39], we also observed decreased intrahepatic macrophage and neutrophil infiltration and alleviated liver injury following ALOX15 inhibition in I/R-insulted liver. A detailed analysis of the structure and organization of the lipoxygenase genes in the human and mouse also suggest that the mouse leukocyte-type 12-LOX (encoded by *Alox15* gene) and the human reticulocyte-type 12/15-LOX (encoded by *ALOX15* gene) are orthologous enzymes[40,41]. Usually, enzyme orthologs fulfill similar functions across various organisms and thus mouse *Alox15* may serve as the functional equivalent of human *ALOX15*[42]. Our results also revealed that recipients with high ALOX15 levels in pre-transplant liver grafts had a significantly higher incidence of EAD after LT, further validating our exploration from mice to humans. These results suggested that the ALOX15/15-HETE axis is a key pathway regulating graft injury in LT. In addition to the protective effects against hepatic

Fig. 4 | Deficiency of FGF21 exacerbated inflammation and activated an excessive innate immune response in mouse liver transplantation. a Wild-type and *Fgf21* KO donor livers in the mouse orthotopic liver transplantation model were harvested, stored for 30 min at 4 °C, and transplanted into wild-type recipient mice. **b** Serum ALT and AST levels for each group after transplantation (n = 4, per group). **c** The 15-HETE level in the livers of each group 6 h after reperfusion (n = 4, per group). **d** The FGF21 level in the serum of each group 6 h after reperfusion (n = 4, per group). **e** Representative TUNEL staining of liver sections from each group (n = 4, per group). **f** Heatmap showing the differential expression of 41 immune markers in 34 cell clusters. **g** Two-dimensional t-SNE illustration of the CyTOF data of livers isolated from WT >> WT and KO >> WT (n = 4/group), the merged t-SNE graph was used for contrast. **h**–**j** The frequencies of the identified clusters in granulocytes, Mono/Mac cells and NK cells and the comparisons between the groups (n = 4, per group), boxplot shows the median (center line), 25th, and 75th percentile (lower and upper boundary), and the whiskers are essentially range bars that extend to max and min values. **k** Multiplex immunohistochemistry staining of NK1.1 (green), CD62L (red) and DAPI (blue) in *Fgf21* KO-transplanted livers, three independent biological mice samples. Scale bar, 50 μm. OLT orthotopic liver transplantation, WT wild-type, KO knockout, ALT, alanine aminotransferase, AST aspartate aminotransferase, TUNEL Terminal deoxynucleotidyl transferase dUTP nick end labeling, Mono/Mac monocyte/macrophage, NK natural killer. Two-tailed t-test. Statistic data are presented as the mean ± SD, error bars represent the means of at least three independent experiments. *p* values are shown on the graphs, $p < 0.05$ was considered statistically significant. Source data are provided as a Source Data file. Figure 4a created with BioRender. com released under a Creative Commons Attribution-NonCommercial-NoDerivs 4.0 International license (https://creativecommons.org/licenses/by-nc-nd/4.0/deed.en).

inflammation and cell injury, Martinez-Clemente et al.'s findings also showed a decrease in hepatic steatosis in $ApoE^{-/-}$ mice lacking *Alox15*[20]. The observed antisteatotic effect is more likely due to a combination of actions on pivotal pathways that drive the progression to hepatic steatosis, notably those associated with insulin resistance. Therefore, to avoid the condition with shAlox15 reflecting more the role of *Alox15* in steatosis formation, we minimized the transfection time to three weeks before I/R injury in steatotic livers.

Innate immune activation is the dominant response in this inflammatory cytotoxic cycle, which eventually transforms an immunologically quiescent milieu into an inflammatory and destructive status[4,43,44]. Our previous study delineated a pro-inflammatory phenotype of macrophages that was enriched in transplanted steatotic livers and potentially participated in fatty graft injury[45]. To better understand the impact of FGF21 on the liver graft immune milieu, CyTOF was used to elucidate the immune landscape of *Fgf21* KO-transplanted livers. FGF21 deficiency aggravated the innate immune response early after transplantation, primarily by activating granulocytes, monocyte-derived macrophages and NK cells. Recent studies documented macrophage- and neutrophil-mediated tissue damage and systemic inflammation in hepatic I/R injury[46,47], but the impact of NK cells is poorly understood. Notably, we identified a predominant cluster of NK cells in *Fgf21* KO -transplanted livers, $CD62L^+$ NK cells, which primarily accumulated around the peripheral portal vein and indicated their recruitment from peripheral blood. Future studies are still necessary to evaluate the efficiency of graft protection via targeting $CD62L^+$ NK cells.

Evidence from clinical and experimental observations suggests that the use of steatotic liver grafts increases the risks of complications after transplantation[48,49]. However, the underlying mechanisms for its vulnerability to I/R injury must be elucidated, which is noteworthy for the development of new therapeutic strategies for steatotic liver grafts. Liu et al. recently found that serum FGF21 was elevated in patients who received steatotic grafts in the early phase (2 h post-LT) or late phase (7 days post-LT)[50]. Pharmacological FGF21 and its analogs improved metabolic status in preclinical models of diabetes and nonalcoholic fatty liver disease (NAFLD)[10,51], which suggests their potential as therapeutic agents for steatotic liver grafts in transplantation. The present study found that higher FGF21 levels were related to decreased graft injury after transplantation in our cohort using steatotic grafts. I/R injury appeared more severe in steatotic livers in vivo, and FGF21 deficiency further increased hepatic injury, lipid accumulation and steatosis after I/R treatment. The regulatory role of the FGF21/ALOX15/15HETE axis was also more significant. Transgenic overexpression of hepatic FGF21 or infusion with rmFGF21 successfully alleviated liver injury, apoptosis and inflammation in steatotic livers after I/R treatment. A clear reversal of I/R-induced intrahepatic lipid accumulation and liver triglyceride contents were also demonstrated in the treated mice.

The potential clinical application of FGF21 in treating steatotic livers is significant. Compared to other defatting strategies, FGF21 has distinctive mechanisms of action and some comparative advantages concerning efficacy, safety, and feasibility, outlined as follows: (1) In addition to alleviating early liver graft injury as reported in our study, the pharmacological administration of FGF21 has also been demonstrated to have multiple beneficial effects in patients with NAFLD/NASH. These benefits include increased hepatic insulin sensitivity, induced fatty acid β-oxidation, inhibition of de novo lipogenesis, and decreased delivery of very-low-density lipoprotein to the liver[10,52]. (2) As a water-soluble drug, FGF21 has advantages over most defatting drugs (lipid-soluble ones) due to their better absorption, uniform distribution, efficient elimination, predictable pharmacokinetics, and safer profile, making them preferable for clinical use in terms of efficacy and safety[53,54]. Therefore, our paradigm of killing two birds with one stone may be interpreted in the preservation and repair of steatotic liver grafts in combination with normothermic machine perfusion.

In conclusion, the present study demonstrated that FGF21 was an effective biomarker for acute graft injury after LT, especially steatotic grafts. FGF21 deficiency disrupted immunometabolic homeostasis via the ALOX15/15-HETE axis in hepatic I/R injury, which aggravated graft injury after LT. Exogenous supplementation with FGF21 may be an effective strategy to mitigate liver graft injury and prevent EAD, particularly transplantations using steatotic liver grafts.

Methods

Ethics approval

This study involved human participants and was approved by Clinical Research Ethics Committee of the First Affiliated Hospital, Zhejiang University School of Medicine (2020–1224). Informed written consent was obtained from all participants as well. Sex and/or gender was determined based on self-reporting. Animal study was approved by the Animal Experimental Ethical Inspection of the First Affiliated Hospital, Zhejiang University School of Medicine (2020–1482).

Clinical liver transplantation procedure

All the included recipients from January 2015 to December 2018 received modified piggyback LT, as specified by The First Affiliated Hospital, Zhejiang University School of Medicine's liver transplant protocols. Recipients who underwent pediatric transplantation, retransplantation or split LT were excluded from this study. The general details of the standard technique and reperfusion method is outlined below. (1) Donor livers, procured from donation after brain death or cardiac death with standardized techniques, were perfused with and stored in cold University of Wisconsin (UW) solution. (2) The procedure in a recipient hepatectomy includes hepatic hilum dissection and full division of the perihepatic ligaments, followed by inferior vena cava (IVC) devascularization. (3) Liver grafts were mainly implanted using a modified piggyback technique: (1) Recipient IVC: according to the patient's hepatic vein anatomy, the hepatic veins (left, middle and right) are split from the middle and trimmed into a continuous

https://doi.org/10.1038/s41467-024-52379-2

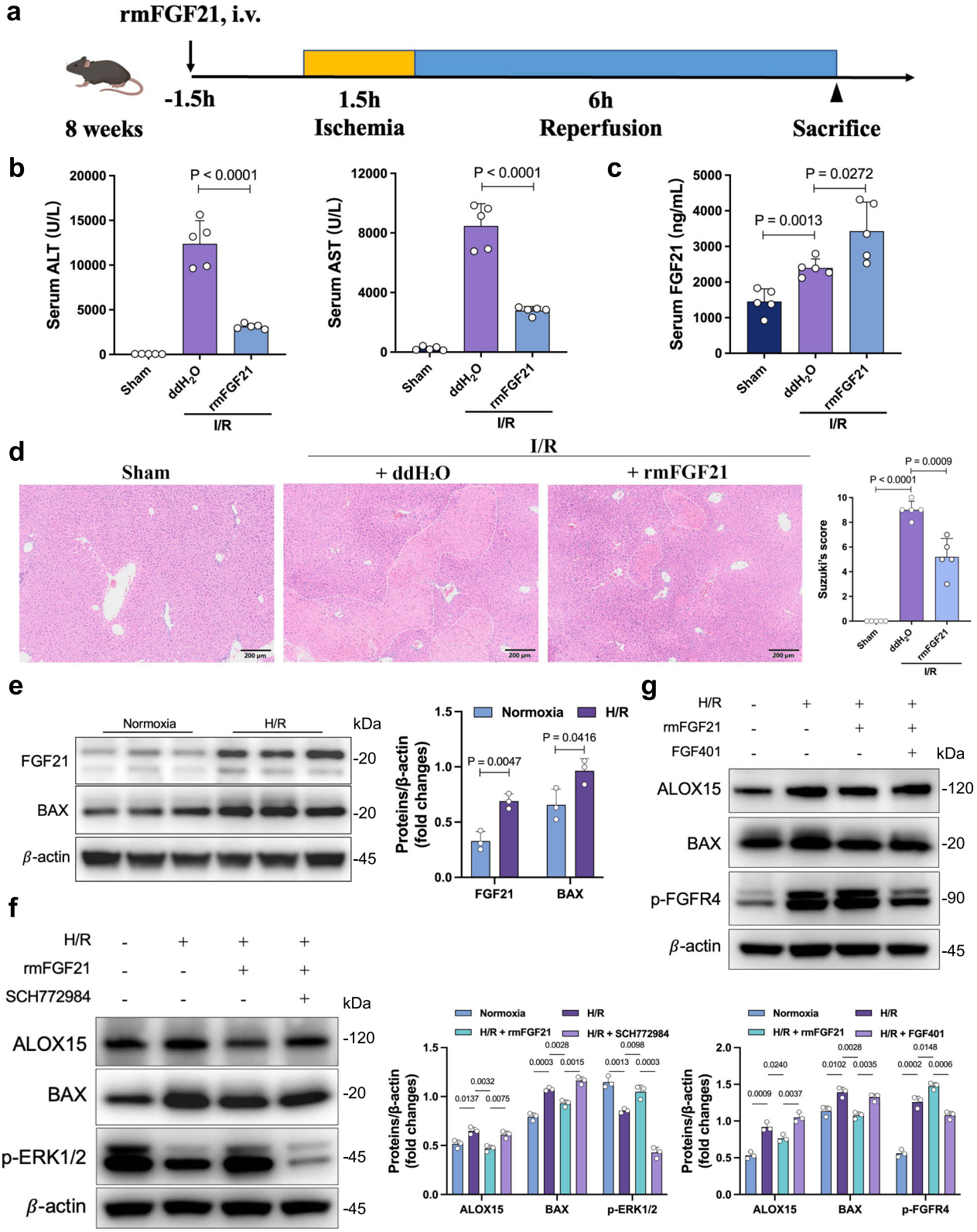

Fig. 5 | Treatment with rmFGF21 relieved I/R-induced hepatocellular injury. **a** Experimental schema for establishing the I/R injury mouse model. The mice were intravenously administered rmFGF21 (0.5 mg/kg). **b** Serum ALT and AST levels 6 h after reperfusion (n = 5, per group). **c** Comparison of serum FGF21 levels 6 h after reperfusion (n = 5, per group). **d** H&E staining of liver sections 6 h after reperfusion (n = 5, per group). **e** Western blot analysis (left) and quantification (right) of FGF21and BAX in AML12 from each group. **f** Western blot analysis (left) and quantification (right) of ALOX15, BAX and p-ERK1/2 in AML12 from each group. **g** Western blot analysis (up) and quantification (down) of ALOX15, BAX and p-FGFR4 in AML12 from each group. **e**–**g** three independent biological mice samples. I/R ischemia/reperfusion, ALT alanine aminotransferase, AST aspartate aminotransferase, H/R hypoxia/ reoxygenation. Two-tailed t-test. Statistic data are presented as the mean ± SD, error bars represent the means of at least three independent experiments. *p* values are shown on the graphs, $p < 0.05$ was considered statistically significant. Source data are provided as a Source Data file. Figure 5a created with BioRender. com released under a Creative Commons Attribution-NonCommercial-NoDerivs 4.0 International license (https://creativecommons.org/licenses/by-nc-nd/4.0/deed.en).

https://doi.org/10.1038/s41467-024-52379-2

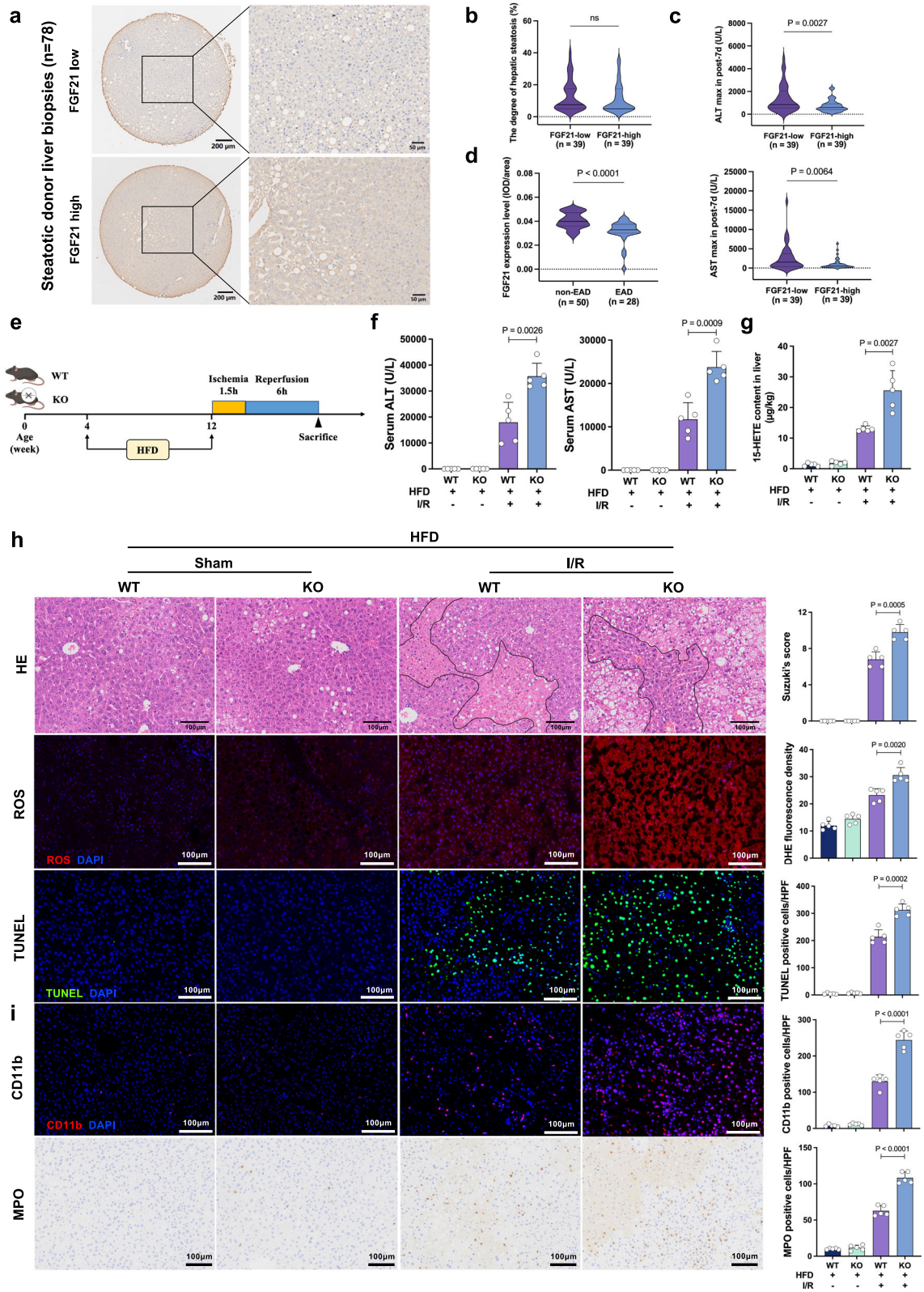

opening, and the front wall of inferior vena cava is also trimmed longitudinally, and all these together form an inverted triangular incision. (2) Donor IVC: the posterior wall of the donor superior inferior vena cava was cut longitudinally with the two up angers of hepatic superior IVC, also trimmed into an inverted triangular incision. (3) these two inverted triangular incisions are anastomosed. (4) Then, the portal vein anastomosis was completed first, followed by the hepatic artery anastomosis. Reperfusion commenced with the unclamping of the portal vein, allowing portal venous blood flow to the liver, followed by unclamping of the hepatic artery. The condition of the bile ducts should be considered when deciding whether to implant a T-tube.

Clinical samples

To detect the dynamic changes in peripheral FGF21 before and 2 h after reperfusion, serum samples were randomly collected from 88 cases

Fig. 6 | FGF21 deficiency further deteriorated I/R injury in steatotic livers. a IHC staining for FGF21 in pre-transplant biopsies from the steatotic liver grafts in Cohort 3 (n = 78). **b** Comparison of the degree of hepatic steatosis between the low FGF21 group and the high FGF21 group. **c** Comparison of maximal serum ALT/AST within 7 days after transplantation between the low FGF21 group and the high FGF21 group. **d** Comparison of FGF21 staining (mean integrated optical density, IOD) between patients who did and did not develop EAD. **e** Schematic for the establishment of the I/R injury model using mice fed a high-fat diet (HFD) or normal chow diet. After 8 weeks of feeding, mice were subjected to I/R treatment. **f** Serum ALT and AST 6 hours after reperfusion (n = 5, per group). **g** 15-HETE content in the livers from each group 6 h after reperfusion (n = 5, per group). **h** H&E staining, ROS staining and TUNEL staining of liver sections from each group 6 h after reperfusion (n = 5, per group). **i** Quantification assessment of infiltrating $CD11b^+$ and MPO^+ cells in the livers from each group (n = 5, per group). I/R ischemia/reperfusion, WT wild-type, KO knockout, HFD high-fat diet, ALT alanine aminotransferase, AST aspartate aminotransferase, HE hematoxylin and eosin, ROS reactive oxygen species, DHE dihydroethidium, TUNEL terminal deoxynucleotidyl transferase dUTP nick end labeling, MPO cytosolic myeloperoxidase. Two-tailed t-test. Statistic data are presented as the mean ± SD, error bars represent the means of at least three independent experiments. *p* values are shown on the graphs, ns, not significant, $p < 0.05$ was considered statistically significant. Source data are provided as a Source Data file. Figure 6e created with BioRender. com released under a Creative Commons Attribution-NonCommercial-NoDerivs 4.0 International license (https://creativecommons.org/licenses/by-nc-nd/4.0/deed.en).

(Cohort 1). Pre-transplant biopsies were obtained from the left liver lobe after liver cold storage at back table (before implantation) from a corresponding 193 cases. Of these, 115 cases (Cohort 2) were enrolled to analyze the general association between FGF21 or ALOX15 and clinical outcomes. Another independent cohort of 78 cases (Cohort 3) was exclusively steatotic and was used to analyze the impact of FGF21 on steatotic grafts. Cold ischemia time (CIT) was defined as the time between the perfusion of the donor liver with UW solution and its removal from the cold storage for implantation. Donor warm ischemia time (DWIT) was defined as the time interval between graft removal from cold storage and the establishment of graft reperfusion. EAD was defined by the presence of one or more of the following variables: (I) total bilirubin (TB) ≥ 10 mg/dL on postoperative day 7; (II) an international normalized ratio (INR) ≥ 1.6 on postoperative day 7, or (III) alanine aminotransferase (ALT) or aspartate aminotransferase (AST) levels >2000 U/L within the first 7 postoperative days[55]. Dynamic FGF21 mRNA expression changes in the liver grafts were analyzed using the GEO Dataset GSE15480 and GSE151648, which contain respectively 12 and 40 pairs of graft biopsies pre-transplantation and post-transplantation (within 2 h post-reperfusion).

The definition of steatosis in liver grafts

Macrovesicular steatosis (MaS) is an important criterion defining extended-criteria donor organs[56]. MaS was defined as a single vacuole, larger than the nucleus, replacing most of the hepatocyte's cytoplasm and displacing the nucleus toward the cytoplasmic border[57]. Hepatic MaS was characterized quantitatively by the percentage of hepatocytes containing lipid droplets, determined by histological examination before implanting into recipients. Hepatic steatosis was categorized as follows: no steatosis (MaS affected less than 5% of hepatocytes), mild (MaS affected 5–29% of hepatocytes), moderate (MaS affected 30–60% of hepatocytes)[7]. Microvesicular steatosis (small droplet macrosteatosis) was not included in determining steatosis percentage.

Animals

Fgf21 KO mice (C57BL/6 background) were purchased from Cyagen Biosciences, Inc (CA, USA). and bred in our facility under specific pathogen-free conditions. Mice homozygous for a knockout allele of *Fgf21* were identified using PCR analyses (F: 5′-CAGACCCAGGAGTGTAGACTTCAG-3′ and R: 5′-CCAGTGGTTCCATTCTCAGTAC-3′) of genomic DNA extracted from mouse toes (Supplementary Fig. 11). C57BL/6 controls were purchased from Zhejiang Academy of Medical Sciences (ZAMS). Male mice aged 4 weeks (weighing 14 to 16 g) or 8 weeks (weighing 22 to 24 g) were divided randomly into the experimental and control groups. Four-week-old male *Fgf21* KO mice and wild type (WT) littermates were fed normal chow diet (10 kcal% fat; D12450J; Research Diets) or high fat diet (60 kcal% fat; D12492; Research Diets) for 8 weeks. Mice were given free access to water and housed under specific pathogen-free conditions at 20–25 °C with 50–70% humidity and a 12 h light/dark cycle. In our study, mice were euthanized using carbon dioxide (CO_2) inhalation.

All animal experiments complied with the principals of the Animals in Research: Reporting In Vivo Experiments (ARRIVE) guidelines, incorporated the 3Rs principal. The Institutional Animal Use and Care Committee of Zhejiang University approved all experimental protocols.

Development of high-fat diet (HFD)-triggered non-alcoholic fatty liver disease

Mice on an HFD regimen were fed a diet containing 60% calories fat (D12492, Research Diets) for 8 weeks to produce moderate fatty liver. The control mice were fed a regular chow diet.

Mouse liver I/R injury model and animal treatment

A model of partial (70%) hepatic warm I/R was used. Briefly, all structures in the portal triad (hepatic artery, portal vein, and bile duct) to the cephalad lobes were clamped with a microvascular clamp for 1.5 h, and reperfusion was initiated by clamp removal. Sham control mice underwent the same procedure without vascular occlusion. Mice in the treatment groups were injected 1.5 h prior to the initiation of hepatic ischemia with a single dose of recombinant murine FGF21 (rmFGF21, 0.5 mg/kg i.v., C04D, Novoprotein), and HFD-fed mice were treated with rmFGF21 (0.5 mg/kg/d, i.p.) for 2 weeks prior to I/R. PD146176 (10 mg/kg i.p., sc-200678A, Santa Cruz) or 15-HETE (0.5 mg/kg i.p., sc-200944, Santa Cruz) in formulated solution (DMSO: PEG300: Tween80: water, 4:30:5:61) was injected 30 min prior to the initiation of hepatic ischemia. Mice were sacrificed 6 h after reperfusion, and ischemic hepatic lobes and serum samples were collected for further analysis.

Mouse orthotopic liver transplantation (OLT)

The mouse model of mouse orthotopic LT was established. Briefly, the donor mice was subjected to anaesthesia and subsequent systemic heparinization. The donor liver detached from the mice was immersed in University of Wisconsin (UW) solution and then was implanted orthotopically into the abdomen of the recipient mice. The anastomosis of the supra- hepatic vena cava was continuously sutured with 10-0 microscopic vascular suture. The cuff technique was applied to connect portal vein and infrahepatic vena cava. After then, the bile duct was re- constructed by an end-to-end anastomosis over an indwelling stent. Hepatic artery was not reconstructed. After OLT, standard rodent chow and sterilized water were available ad libitum. Donor livers (WT or *Fgf21* KO; C57BL/6) were transplanted to syngeneic, rather than allogeneic, recipient mice. Liver graft and serum were collected 6 h after reperfusion, which is the peak of hepatocellular damage in this model. The sham group underwent the same procedures except for OLT.

In vitro hypoxia/reoxygenation (H/R) model

AML12 cells, a non-tumorigenic mouse hepatocyte cell line, were obtained from Shanghai Anwei-sci Cell Center (# AW-CELLS-M0074) and cultured in DMEM/F12 containing 0.005 mg/mL insulin, 0.005 mg/mL transferrin, 5 ng/mL selenium, 40 ng/mL dexamethasone and 10 % FBS at standard cell culture conditions (5% CO_2, 95 % air). In order to establish

https://doi.org/10.1038/s41467-024-52379-2

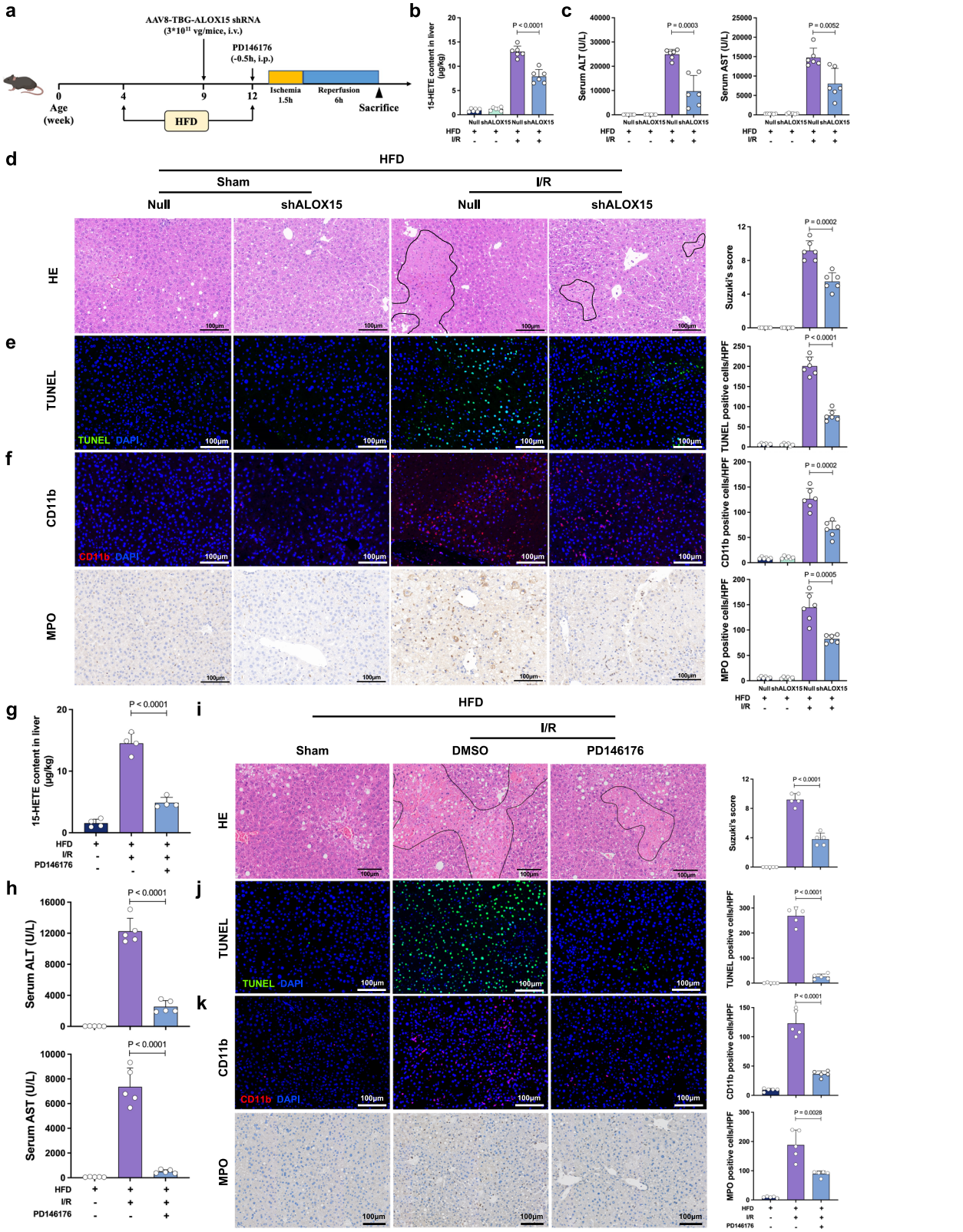

an in vitro ischemia reperfusion model, the AML12 were cultured with serum-free DMEM in a humidity airtight chamber equilibrated with 94% N_2-5%CO_2-1%O_2 for hypoxia training for 12 h. The medium was then replaced with reoxygenation medium, and cells were further incubated at 37 °C in a 95%O_2-5%CO_2 atmosphere for another 6 h. In the AML12 cells H/R assay, PD-166866 (0.1 μM, MedChemExpression, HY-101296), FGF-401 (10 nM, HY-101568), SCH772984 (0.1 μM, HY-50846) and LY294002 (1 μM, HY-10108) were used to inhibit the expression of FGFR1, FGFR4, ERK 1/2, and PI3K, respectively. The cells were pretreated with inhibitors at indicated concentrations before the H/R procedure. AML12 cells were also pretreated with rmFGF21 (1 ug/mL) before the H/R procedure.

Fig. 7 | The ALOX15-15-HETE axis in I/R injury in steatotic livers. a The steatotic mouse models were treated with AAV8-TBG-*Alox15* shRNA (shAlox15) or PD146176 prior to I/R treatment. **b** 15-HETE content in the livers from the Sham group, Control group and shAlox15 group 6 h after reperfusion (n = 6, per group). **c** Serum ALT and AST levels for the Sham group, Control group and shAlox15 group 6 h after reperfusion (n = 6, per group). **d** H&E staining of liver sections from the Sham group, Control group and shAlox15 group 6 h after reperfusion (n = 6, per group). **e** TUNEL immunofluorescent staining in liver lobes of the Sham group, Control group and shAlox15 group 6 h after reperfusion (n = 6, per group). **f** CD11b and MPO IHC staining of liver sections from the Sham group, Control group and shAlox15 group 6 h after reperfusion (n = 6, per group). **g** 15-HETE content in the livers from the Sham group, Control group and PD146176 group 6 h after reperfusion (n = 5, per group). **h** Serum ALT and AST levels of the Sham group, Control group and PD146176 group 6 h after reperfusion (n = 5, per group). **i** H&E staining of liver sections from the Sham group, Control group and PD146176 group 6 h after reperfusion (n = 5, per group). **j** TUNEL immunofluorescent staining in liver lobes of the Sham group, Control group and PD146176 group 6 h after reperfusion (n = 5, per group). **k** CD11b and MPO IHC staining of liver sections from the Sham group, Control group and PD146176 group 6 h after reperfusion (n = 5, per group). I/R, ischemia/reperfusion; WT, wild-type; KO, knockout; HFD, high-fat diet; ALT, alanine aminotransferase; AST, aspartate aminotransferase; HE, hematoxylin and eosin; TUNEL, terminal deoxynucleotidyl transferase dUTP nick end labeling; MPO, cytosolic myeloperoxidase. Two-tailed t-test. Statistic data are presented as the mean ± SD, error bars represent the means of at least three independent experiments. *p* values are shown on the graphs, $p < 0.05$ was considered statistically significant. Source data are provided as a Source Data file. Figure 7a created with BioRender. com released under a Creative Commons Attribution-NonCommercial-NoDerivs 4.0 International license (https://creativecommons.org/licenses/by-nc-nd/4.0/deed.en).

Serum transaminase assay and lipid detection

Mouse serum alanine transaminase (ALT), aspartate aminotransferase (AST) and triglyceride (TG) levels were detected using a fully automatic biochemical analyzer (BS-220; Mindray).

RNA-seq and data processing

After the extraction of total RNA, mRNA was isolated using Oligo Magnetic Beads. Libraries were generated using the NEBNext UltraTM RNA Library Prep Kit (BGI-Tech, Shenzhen, China) for the Illumina system following the manufacturer's instructions. Sequencing was performed using the Illumina HiSeq XTEN platform. Differential gene expression and statistical significance were analyzed using DESeq2 software. Differentially expressed genes (DEGs) were screened based on set criteria: $|Log2FC| > 1.5$ and false discovery rate (FDR) < 0.05.

Lipidomics

Lipidomics was performed by Metware (Wuhan, China) to analyze the differential lipidomics profiling in twelve livers from mice (n = 4 per group, C57BL/6 background). Briefly, 80 µL ultrapure water and 200 µL methanol/acetonitrile solution containing internal standard were added into the cell sample and vortexed for 5 min. The protein was precipitated at low temperature (−20 °C) for 30 min. The sample was centrifuged at 12,000 rpm for 10 min (4 °C). The all supernatant was collected and transferred. The eicosanoids in supernatants were extracted using Poly-Sery MAX SPE columns (ANPEL). Prior to analysis, the eluent was dried under vacuum and redissolved in 100 µL of methanol/water for UPLC/MS/MS analysis. The sample extracts were analyzed using an LC-ESI-MS/MS system (UPLC, ExionLC AD, SCIEX; MS, QTRAP® 6500+ System, SCIEX). The analytical conditions were as follows, HPLC: column, Waters ACQUITY UPLC HSS T3 C18 (100 mm × 2.1 mm i.d., 1.8 µm); solvent system, water with 0.04% acetic acid (A), acetonitrile with 0.04% acetic acid (B); The gradient was 0–2.0 min from 0.1% to 30% B; 2.0–4.0 min to 50% B; 4.0–5.5 min to 99% B, which was maintained for 1.5 min; and 6.0–7.0 min reduced to 0.1% B and maintained for 3.0 min. flow rate, 0.4 mL/min; temperature, 40 °C; injection volume: 10 µL. Linear ion trap (LIT) and triple quadrupole (QQQ) scans were acquired on a triple quadrupole-linear ion trap mass spectrometer (QTRAP), QTRAP® 6500 + LC-MS/MS System, equipped with an ESI Turbo Ion-Spray interface, operating in negative ion mode and controlled by Analyst 1.6.3 software (SCIEX). The ESI source operation parameters were as follows: ion source, ESI-; source temperature 550 °C; ion spray voltage (IS) −4500 V; curtain gas (CUR) was set at 35 psi, respectively. Eicosanoids were analyzed using scheduled multiple reaction monitoring. Data acquisitions were performed using Analyst 1.6.3 software. Multiquant 3.0.3 software (SCIEX) was used to quantify all metabolites. Mass spectrometer parameters including the declustering potentials (DP) and collision energies (CE) for individual MRM transitions were done with further DP and CE optimization. A specific set of MRM transitions were monitored for each period according to the metabolites eluted within this period.

Cytometry by time-of-flight (CyTOF)

CyTOF was performed by PLTTech Inc. (Hangzhou, China) to analyze the differential immune cellular profiling in eight transplanted livers from mice (n = 4 per group, C57BL/6 background). Briefly, mouse liver tissue was dissociated into single cells using DNase, collagenase IV and hyaluronidase (Sigma-Aldrich, St. Louis, MO, USA). Immune cells were enriched using Percoll density gradient media (Sigma-Aldrich), and red blood cells were removed using ACK Lysing Buffer (Sigma-Aldrich). Qualified samples were blocked and stained for 30 min with a panel of 42 antibodies (Supplementary Table 4), followed by fixation overnight. Permeabilization buffer was applied, and the cells were incubated in an intracellular antibody mix. The cells were rinsed, and the signals were detected using a CyTOF system (Helios, Fluidigm, CA, USA). The types of immune cells were identified via nonlinear dimensionality reduction [t-distributed stochastic neighbor embedding (tSNE)], followed by density clustering.

Inflammatory profiling of post-transplant liver tissues and blood samples

Liver tissues and plasma were obtained and diluted in Bio-Plex Sample Diluent HB buffer for inflammatory profiling. Then the diluted plasma samples were analyzed via a Bio-Plex Pro Mouse Cytokine Panel 23-Plex assay (Bio-Rad, Cat# 64209360) per the manufacturer's instructions. The samples were analyzed using the Bio-Plex system and Bio-Plex Manager software with 5PL curve fitting (Bio-Rad Laboratories). The reader was set to read a minimum of 200 beads, and the results were expressed as median fluorescence intensity.

Construction and administration of AAV8 vectors

AAV8 vectors encoding codon-optimized murine *Fgf21* under the control of the human alpha 1-anti-trypsin (hAAT) promoter (AAV8-hAAT-*Fgf21* vectors) were generated in the laboratory of GENECHEM according to a previously described method[58]. A noncoding plasmid carrying the hAAT promoter was used to produce null particles (AAV8-hAAT-null). AAV8-TBG-*Alox15* shRNA was procured from WZ Biosciences Inc. for gene silencing. For systemic administration, AAV8 vectors were administered via tail vein injection at a dose of 2×10^{11} vg/mouse for AAV8-hAAT-*Fgf21* or 3×10^{11} vg/mouse for AAV8-TBG-*Alox15* shRNA in a total volume of 200 µl. Mice were fed an HFD diet after administration and maintained for eight weeks.

The enzyme-linked immunosorbent assay (ELISA) for recipient's serum

The human FGF21 ELISA kit (EHC146; Neobioscience, China), Mouse/Rat FGF-21 ELISA Kit (MF2100; R&D Systems, USA) and HMGB1 ELISA kit (NBP2-62766; Novus Biologicals, USA) were used to detect the

https://doi.org/10.1038/s41467-024-52379-2

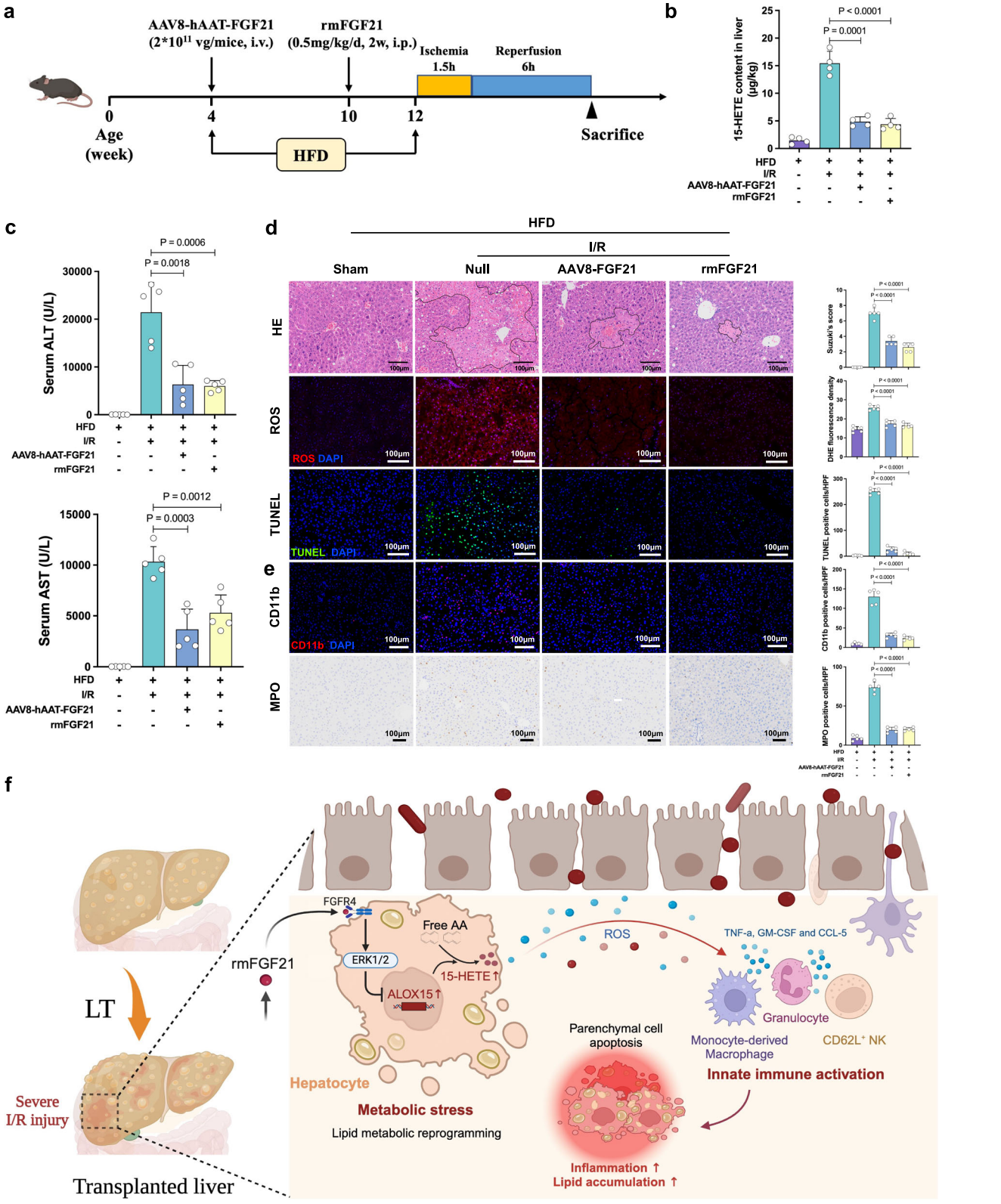

serum FGF21 and HMGB1 levels according to the manufacturer's introduction. The 96-well plate was precoated with antibody. The human serum samples (100 μL/well) were added into the wells and the plate was incubated for 1.5 h at 37 °C. The plate was washed for 5 times with washing buffer. Then secondary antibody conjugated with HRP was added to the wells for 1 h incubation at 37 °C in the dark. After formation of the antibody-antigen-enzyme-labeled antibody complex, the substrate TMB was added after thorough washing. To stop the reaction, add 100 μL stop solution to each well. Finally, the plate was read at 450 nm in an absorbance microplate reader. Standard curve was made with the standard samples and all experimental values were calculated based on the standard curve.

H&E staining and immunohistochemical staining

The human donor graft tissues from LT surgery and mouse liver tissues from hepatic I/R injury and LT were collected. Tissue samples were

Fig. 8 | Transgenic overexpression of hepatic *Fgf21* or administration of rmFGF21 alleviated hepatic I/R injury in steatotic livers. a The steatotic mouse models underwent intravenous injection of rmFGF21 (0.5 mg/kg) or tail vein injection of AAV8-hAAT-*Fgf21* before I/R injury. **b** 15-HETE content in the livers from each group 6 h after reperfusion (n = 4, per group). **c** Serum ALT and AST 6 h after reperfusion (n = 5, per group). **d** H&E staining, ROS staining and TUNEL staining and quantification results of liver sections from each group 6 h after reperfusion (n = 5, per group). **e** Quantification assessment of infiltrating $CD11b^+$ and MPO^+ cells in the livers of each group (n = 5, per group). **f** The general schematic diagram. LT, liver transplantation; AA, arachidonic acid. I/R, ischemia/reperfusion; HFD, high-fat diet; ALT, alanine aminotransferase; AST, aspartate aminotransferase; HE, hematoxylin and eosin; ROS, reactive oxygen species; DHE, dihydroethidium; TUNEL, terminal deoxynucleotidyl transferase dUTP nick end labeling; MPO, cytosolic myeloperoxidase. Two-tailed t-test. Statistic data are presented as the mean ± SD, error bars represent the means of at least three independent experiments. *p* values are shown on the graphs, $p < 0.05$ was considered statistically significant. Source data are provided as a Source Data file. Figure 8a, f created with BioRender. com released under a Creative Commons Attribution-NonCommercial-NoDerivs 4.0 International license (https://creativecommons.org/licenses/by-nc-nd/4.0/deed.en).

fixed with formalin and embedded with paraffin. To assess the necrosis of the liver, hematoxylin and eosin (H&E) staining was performed and evaluated as previously reported[59]. For IHC staining, paraffin sections were stained by immunofluorescence as previously reported[60]. Primary antibodies against FGF21 (ab171941, Abcam), CD11b (14-0112-85, Invitrogen) and MPO (22225-1-AP, Proteintech) were used. Liver sections were evaluated from 10 high-power randomly-selected fields. Positive cell counts were determined by Image-Pro Plus software (version 6.0).

NAFLD Activity Score (NAS)

The severity of steatosis, lobular inflammation and hepatocellular ballooning were scored using the NASH-Clinical Research Network (CRN) criteria[61]. Briefly, the NAS score incorporates pathologist's interpretation of important features of NAFLD and scores for steatosis (0–3), ballooning (0–2) and inflammation (0–3) for a score out of 8.

TUNEL assay

Cell death in liver sections (5 μm) was detected by In Situ Cell Death Detection Kit, Fluorescein (11684795910, Roche) according to the manufacturer's protocol. Briefly, the tissue slides were incubated with 1 μg/mL proteinase K for 15 min at room temperature. After 2 times of PBS washes, the slides were incubated with TUNEL solution for 60 min at 37 °C in the dark. The slides were then washed with PBS for 3 times followed by incubation with a chromogenic HRP substrate solution for 30 min at room temperature. Results were scored semi-quantitatively by blindly counting the number of positive cells in 10 HPF/section (x200).

Detection of reactive oxygen species (ROS) production by fluorescence microscopy

Dihydroethidium (DHE, HY-D0079, MCE) was used to assess ROS production by detecting the fluorescent oxidation product. In brief, the stock solution of DHE was made by dissolving 5 mg of the dye in 1 mL of water; for staining, it was diluted to 5 μg/mL in PBS (1:1000). Slides with frozen liver sections were washed in PBS and incubated with DHE for 30 min at 37 °C. Fluorescence signals were detected by microplate reader at excitation/emission of 510-560/590 nm.

Western blotting analysis

Western blotting was carried out using established protocols as previously described. Briefly, protein concentrations in all the samples were determined by the BCA protein assay kit (# 23227, Thermo Fisher Scientific, UK). Then, proteins were separated using 4%–20% SurePAGE precast gels (# M00657, GeneScript, Shanghai, China) and transferred to 0.45 μm polyvinylidene difluoride (PVDF) membranes (MerckMillipore, Billerica, MA, USA). Next, the membranes were blocked for 30 min with Protein Free Rapid Blocking Buffer (# LA10964, EpiZyme, Shanghai, China) to prevent nonspecific binding. They were then incubated overnight at 4 °C with primary antibodies. Horseradish peroxidase-conjugated secondary antibodies (anti-mouse IgG or anti-rabbit IgG) were applied to the membranes and incubated for 1 h at room temperature. After using an enhanced chemiluminescence substrate, the blots were analyzed with chemiluminescence detection system (Amersham™ Imager 680, Sweden). All primary and secondary antibodies used in experiments were listed in Supplementary Table 5.

Statistical analyses

All statistical analyses and graphing were performed using SPSS (Version 26.0, Inc., IL, USA) and Prism 8 (GraphPad Software, CA). Cumulative survival rates were estimated using the Kaplan–Meier method, and survival curves were compared using log-rank tests. Continuous variables are expressed as the mean ± standard deviation (SD) or median and interquartile range (25th and 75th centiles) depending on the distribution. Categorical variables are presented as absolute values and percentages (%). Continuous variables were compared using Student's *t* test or Mann–Whitney U test when the variables were not normally distributed. Categorical variables were compared using Pearson's chi-square test or Fisher's exact test. In vitro and in vivo experiments were done with at least three biological replicates per condition, except for RNA-seq, metabolomics and CyTOF, which were performed once. However, at least four biologically independent samples per group were measured in the omics profiling. Differences in values were considered significant at $p < 0.05$.

Reporting summary

Further information on research design is available in the Nature Portfolio Reporting Summary linked to this article.

Data availability

The previously published RNA-seq data of GEO, GSE15480 and GSE151648 were used in this paper. The raw data of RNA-seq in this study have been deposited in the Genome Sequence Archive (GSA) under accession code CRA018064. The original flow cytometry standard data files from CyTOF have been deposited at FigShare with https://doi.org/10.6084/m9.figshare.26403022.v1 (https://figshare.com/articles/dataset/CyTOF_of_mouse_liver_transplantation_samples_from_FGF21_KO_and_wild-type_mice/26403022). The Lipidomics data generated in this study are provided in Source Data file. The remaining data are available within the Article, Supplementary Information or Source Data file. Source data are provided with this paper. All data supporting the findings described in this manuscript are also available from the corresponding author upon request. Source data are provided with this paper.

References

1. Wang, K. et al. Severity of early allograft dysfunction following donation after circulatory death liver transplantation: a multicentre study. *Hepatobiliary Surg. Nutr.* **10**, https://doi.org/10.21037/hbsn.2019.09.02 (2021).
2. Agopian, V. et al. Multicenter validation of the liver graft assessment following transplantation (L-GrAFT) score for assessment of early allograft dysfunction. *J. Hepatol.* https://doi.org/10.1016/j.jhep.2020.09.015 (2020).
3. Bastos-Neves, D., Salvalaggio, P. Rd. O. & Almeida, M. D. Risk factors, surgical complications and graft survival in liver transplant recipients with early allograft dysfunction. *Hepatobiliary Pancreatic Dis. Int.* **18**, 423–429 (2019).

4. Hirao, H., Nakamura, K. & Kupiec-Weglinski, J. W. Liver ischaemia-reperfusion injury: a new understanding of the role of innate immunity. *Nat. Rev. Gastroenterol. Hepatol.* https://doi.org/10.1038/s41575-021-00549-8 (2021).
5. Li, Z.-W. & Wang, L. The role of liver sinusoidal endothelial cells in liver remodeling after injury. *Hepatobiliary Pancreatic Dis. Int.* **22**, 22–27 (2023).
6. Zhang, T. et al. Trends in Outcomes for Marginal Allografts in Liver Transplant. *JAMA Surg.* https://doi.org/10.1001/jamasurg.2020.2484 (2020).
7. Croome, K. et al. Perioperative and long-term outcomes of utilizing donation after circulatory death liver grafts with macrosteatosis: a multicenter analysis. *Am. J. Transplant.* **20**, 2449–2456 (2020).
8. Jackson, K. R. et al. Outcomes after declining a steatotic donor liver for liver transplant candidates in the United States. *Transplantation* **104**, 1612–1618 (2020).
9. Flippo, K. H. & Potthoff, M. J. Metabolic messengers: FGF21. *Nat. Metab.* **3**, 309–317 (2021).
10. Geng, L., Lam, K. & Xu, A. The therapeutic potential of FGF21 in metabolic diseases: from bench to clinic. *Nat. Rev. Endocrinol.* https://doi.org/10.1038/s41574-020-0386-0 (2020).
11. Sanyal, A. et al. Pegbelfermin (BMS-986036), a PEGylated fibroblast growth factor 21 analogue, in patients with non-alcoholic steatohepatitis: a randomised, double-blind, placebo-controlled, phase 2a trial. *Lancet* **392**, 2705–2717 (2019).
12. Ma, Y. et al. FGF21 attenuates neuroinflammation following subarachnoid hemorrhage through promoting mitophagy and inhibiting the cGAS-STING pathway. *J. Transl. Med.* **22**, 436 (2024).
13. Zhang, I. W. et al. Mitochondrial dysfunction governs immunometabolism in leukocytes of patients with acute-on-chronic liver failure. *J. Hepatol.* **76**, https://doi.org/10.1016/j.jhep.2021.08.009 (2022).
14. Kuhn, H. et al. The evolutionary hypothesis of reaction specificity of mammalian ALOX15 orthologs. *Prog. Lipid Res.* **72**, 55–74 (2018).
15. Heinrich, L., Booijink, R., Khurana, A., Weiskirchen, R. & Bansal, R. Lipoxygenases in chronic liver diseases: current insights and future perspectives. *Trends Pharmacol. Sci.* **43**, 188–205 (2022).
16. Singh, N. K. & Rao, G. N. Emerging role of 12/15-Lipoxygenase (ALOX15) in human pathologies. *Prog. Lipid Res.* **73**, 28–45 (2019).
17. Markworth, J. F. et al. Arachidonic acid supplementation modulates blood and skeletal muscle lipid profile with no effect on basal inflammation in resistance exercise trained men. *Prostaglandins Leukot Essent Fatty Acids* **128**, 74–86 (2018).
18. Hall, Z. et al. Lipid zonation and phospholipid remodeling in non-alcoholic fatty liver disease. *Hepatology* **65**, 1165–1180 (2017).
19. Lazic, M. et al. Reduced dietary omega-6 to omega-3 fatty acid ratio and 12/15-lipoxygenase deficiency are protective against chronic high fat diet-induced steatohepatitis. *PloS ONE* **9**, e107658 (2014).
20. Martínez-Clemente, M. et al. Disruption of the 12/15-lipoxygenase gene (Alox15) protects hyperlipidemic mice from nonalcoholic fatty liver disease. *Hepatology* **52**, 1980–1991 (2010).
21. Zhang, W., Zhong, W., Sun, Q., Sun, X. & Zhou, Z. Hepatic overproduction of 13-HODE due to ALOX15 upregulation contributes to alcohol-induced liver injury in mice. *Sci. Rep.* **7**, 8976 (2017).
22. Magnusson, L. U. et al. High expression of arachidonate 15-lipoxygenase and proinflammatory markers in human ischemic heart tissue. *Biochem. Biophys. Res. Commun.* **424**, 327–330 (2012).
23. Croon, M. et al. FGF21 modulates mitochondrial stress response in cardiomyocytes only under mild mitochondrial dysfunction. *Sci. Adv.* **8**, eabn7105 (2022).
24. Ou, Y., Wang, S.-J., Li, D., Chu, B. & Gu, W. Activation of SAT1 engages polyamine metabolism with p53-mediated ferroptotic responses. *Proc. Natl Acad. Sci. USA* **113**, E6806–E6812 (2016).
25. Arbonés, M. L. et al. Lymphocyte homing and leukocyte rolling and migration are impaired in L-selectin-deficient mice. *Immunity* **1**, 247–260 (1994).
26. Shen, W. et al. FGF21-mediated autophagy: remodeling the homeostasis in response to stress in liver diseases. *Genes Dis.* **11**, 101027 (2024).
27. Kurosu, H. et al. Tissue-specific expression of betaKlotho and fibroblast growth factor (FGF) receptor isoforms determines metabolic activity of FGF19 and FGF21. *J. Biol. Chem.* **282**, 26687–26695 (2007).
28. European Association for the Study of the Liver. EASL clinical practice guidelines: liver transplantation. *J. Hepatol.* **64**, 433–485 (2016).
29. Dar, W. A., Sullivan, E., Bynon, J. S., Eltzschig, H. & Ju, C. Ischaemia reperfusion injury in liver transplantation: Cellular and molecular mechanisms. *Liver Int.* **39**, 788–801 (2019).
30. Zhang, Y. et al. The role of FGF21 in the pathogenesis of cardiovascular disease. *Chin. Med. J.* **134**, 2931–2943 (2021).
31. Kim, C. S. et al. Deficiency of fibroblast growth factor 21 aggravates obesity-induced atrophic responses in skeletal muscle. *J. Inflamm.* **16**, 17 (2019).
32. Wang, D. et al. FGF21 alleviates neuroinflammation following ischemic stroke by modulating the temporal and spatial dynamics of microglia/macrophages. *J. Neuroinflamm.* **17**, 257 (2020).
33. Nishimura, T., Nakatake, Y., Konishi, M. & Itoh, N. Identification of a novel FGF, FGF-21, preferentially expressed in the liver. *Biochim. Biophys. Acta* **1492**, 203–206 (2000).
34. Markan, K. R. et al. Circulating FGF21 is liver derived and enhances glucose uptake during refeeding and overfeeding. *Diabetes* **63**, 4057–4063 (2014).
35. Ye, D. et al. Circulating Fibroblast Growth Factor 21 is a sensitive biomarker for severe ischemia/reperfusion injury in patients with liver transplantation. *Sci. Rep.* **6**, 19776 (2016).
36. Han, H. et al. Danger signals in liver injury and restoration of homeostasis. *J. Hepatol.* https://doi.org/10.1016/j.jhep.2020.04.033 (2020).
37. Monga, S. P. Lipid metabolic reprogramming in hepatic ischemia-reperfusion injury. *Nat. Med.* **24**, 6–7 (2018).
38. Queck, A. et al. Alox12/15 deficiency exacerbates, while Lipoxin A4 Ameliorates hepatic inflammation in murine alcoholic hepatitis. *Front. Immunol.* **11**, 1447 (2020).
39. Wang, W. et al. Single-cell profiling identifies mechanisms of inflammatory heterogeneity in chronic rhinosinusitis. *Nat. Immunol.* https://doi.org/10.1038/s41590-022-01312-0 (2022).
40. Watanabe, T. & Haeggström, J. Z. Rat 12-lipoxygenase: mutations of amino acids implicated in the positional specificity of 15- and 12-lipoxygenases. *Biochem. Biophys. Res. Commun.* **192**, 1023–1029 (1993).
41. Pekárová, M., Kuhn, H., Bezáková, L., Ufer, C. & Heydeck, D. Mutagenesis of triad determinants of rat Alox15 alters the specificity of fatty acid and phospholipid oxygenation. *Arch. Biochem. Biophys.* **571**, 50–57 (2015).
42. Ivanov, I., Kuhn, H. & Heydeck, D. Structural and functional biology of arachidonic acid 15-lipoxygenase-1 (ALOX15). *Gene* **573**, https://doi.org/10.1016/j.gene.2015.07.073 (2015).
43. Eltzschig, H. K. & Eckle, T. Ischemia and reperfusion-from mechanism to translation. *Nat. Med.* **17**, 1391–1401 (2011).
44. Su, X. et al. NLRP3 inflammasome: a potential therapeutic target to minimize renal ischemia/reperfusion injury during transplantation. *Transpl. Immunol.* **75**, 101718 (2022).
45. Yang, X. et al. Single-cell profiling reveals distinct immune phenotypes that contribute to ischaemia-reperfusion injury after steatotic liver transplantation. *Cell Prolif.* **54**, e13116 (2021).
46. Huang, D. Q., El-Serag, H. B. & Loomba, R. Global epidemiology of NAFLD-related HCC: trends, predictions, risk factors and prevention. *Nat. Rev. Gastroenterol. Hepatol.* **18**, 223–238 (2021).

47. Cheng, M.-X. et al. VEGF-C attenuates ischemia reperfusion injury of liver graft in rats. *Transpl. Immunol.* **54**, 59–64 (2019).
48. Croome, K. P. et al. Does Donor Allograft Microsteatosis Matter? Comparison of outcomes in liver transplantation with a propensity-matched cohort. *Liver Transpl.* **25**, 1533–1540 (2019).
49. Miyachi, Y. et al. Etiology of liver steatosis influences the severity of ischemia/reperfusion injury and survival after liver transplantation in rats. *Liver Transpl.* **26**, 1504–1515 (2020).
50. Liu, J. et al. Compromised AMPK-PGC1α axis exacerbated steatotic graft injury by dysregulating mitochondrial homeostasis in living donor liver transplantation. *Annal. Surg.* **276**, e483–e492 (2022).
51. Harrison, S. A. et al. Efruxifermin in non-alcoholic steatohepatitis: a randomized, double-blind, placebo-controlled, phase 2a trial. *Nat. Med.* **27**, 1262–1271 (2021).
52. Harrison, S. A., Rolph, T., Knot, M. & Dubourg, J. FGF21 agonists: an emerging therapeutic for metabolic dysfunction-associated steatohepatitis and beyond. *J. Hepatol.* https://doi.org/10.1016/j.jhep.2024.04.034 (2024).
53. Pouton, C. W. Formulation of poorly water-soluble drugs for oral administration: physicochemical and physiological issues and the lipid formulation classification system. *Eur. J. Pharm. Sci.* **29**, 278–287 (2006).
54. Williams, H. D. et al. Strategies to address low drug solubility in discovery and development. *Pharmacol. Rev.* **65**, 315–499 (2013).
55. Olthoff, K. M. et al. Validation of a current definition of early allograft dysfunction in liver transplant recipients and analysis of risk factors. *Liver Transplant.* **16**, 943–949 (2010).
56. Yersiz, H. et al. Assessment of hepatic steatosis by transplant surgeon and expert pathologist: a prospective, double-blind evaluation of 201 donor livers. *Liver Transplant.* **19**, 437–449 (2013).
57. Frongillo, F. et al. Quantification of degree of steatosis in extended criteria donor grafts with standardized histologic techniques: implications for graft survival. *Transplant. Proc.* **41**, 1268–1272 (2009).
58. Jimenez, V. et al. FGF21 gene therapy as treatment for obesity and insulin resistance. *EMBO Mol. Med.* **10**, https://doi.org/10.15252/emmm.201708791 (2018).
59. Suzuki, S., Toledo-Pereyra, L. H., Rodriguez, F. J. & Cejalvo, D. Neutrophil infiltration as an important factor in liver ischemia and reperfusion injury. Modulating effects of FK506 and cyclosporine. *Transplantation* **55**, 1265–1272, (1993).
60. Zhuo, J. et al. The distinct responsiveness of cytokeratin 19-positive hepatocellular carcinoma to regorafenib. *Cell Death Dis.* **12**, 1084 (2021).
61. Kleiner, D. E. et al. Design and validation of a histological scoring system for nonalcoholic fatty liver disease. *Hepatology* **41**, 1313–1321 (2005).

Acknowledgements

This study was supported by the State Key Program of National Natural Science Foundation of China (No. 81930016 to X.X.); National Key Research and Development Program of China (No. 2021YFA1100500 to X.X.); The Major Research Plan of the National Natural Science Foundation of China (No.92159202 to X.X.); National Natural Science Foundation of China (No. 82370662 to D.L.); National Natural Science Foundation of China (No. 82400765 to X.Y.); The China Postdoctoral Science Foundation (No. 2024M750707 to X.Y.); Projects of Medical and Health Technology Program in Zhejiang Province (WKJ-ZJ-2120 to Q.W.); Key R&D Program of Zhejiang (2022C03108 to J.C.); Projects of Medical and Health Technology Program in Zhejiang Province (2021434810 to X.Z.). We would like to extend our gratitude to Prof. Xiaokun Li and his team for their invaluable constructive comments. All schemes of experiment designs were created with https://www.biorender.com.

Author contributions

X.X., D.L. - study concept/design; X.Y., H.C., W.S., Y.C., R.W. - experimental data acquisition; X.Y., H.C., W.S., Y.C., Z.Lian., J.Z., Z.H., C.L. - surgical procedures; X.Y., H.C., Modan.Y., H.L., C.H., X.Z., L.X., B.P., Mengfan.Y. - clinical data analyses; X.L., X.W., Q.W., H.X., S.Z., S.W., J.C., Z.Lin. - manuscript review; X.Y., H.C., D.L. - drafted manuscript; X.X., D.L. - obtained funding; all authors have read and commented on the manuscript.

Competing interests

The authors declare no competing interests.

Additional information

Supplementary information The online version contains supplementary material available at https://doi.org/10.1038/s41467-024-52379-2.

Correspondence and requests for materials should be addressed to Di Lu or Xiao Xu.

Peer review information *Nature Communications* thanks Marion Peyrou, Carlo Pulitano and the other anonymous reviewer(s) for their contribution to the peer review of this work. A peer review file is available.